Doctoral Dissertation

Fabrication of Poly(ethylene-*co*-vinyl alcohol) Monoliths *via* Thermally Induced Phase Separation and Their Applications

熱誘起相分離を利用したエチレン－ビニルアルコール共重合体モノリスの作製と応用

Guowei Wang

July 2015

Graduate School of Engineering
Osaka University

Contents

Chapter 3

One-pot fabrication of palladium nanoparticles captured in mesoporous polymeric monoliths and their catalytic application in C-C coupling reactions

Chapter 4

Immobilization of catalase onto hydrophilic poly(ethylene-*co*-vinyl alcohol) monoliths

Chapter 5

Facile fabrication of mesoporous poly(ethylene-*co*-vinyl alcohol)/chitosan blend monoliths

General introduction

Monoliths are versatile functional materials with a three dimensionally continuous porous structure in a single piece [1-2]. Because of their continuous pore structure, tough skeleton, and high surface area, monoliths could enable the fast mass transfer of reagent solutions, showing great potential for various fascinating applications. With the increasing requirement for sustainable development, monoliths will attract more academic and industrial interests. Based on the raw materials, monoliths can be divided to polymer monoliths, carbon monoliths, silica monoliths, ceramic monoliths, and metal monoliths.

Polymer monoliths have been widely developed since the first paper published by Ŝvec and Fréchet [2]. They mainly used the polymer monoliths as separation columns in chromatography. In the early age of chromatography, the columns were prepared by packing small particles which are useful as stationary phase for the pass-through of mobile phase (organic solvent, water, etc). However, the particle-packed columns faced the problems such as low efficiency for large molecules, high back-pressure, and excess interstitial voids. The monoliths with continuous pore structures and high permeability could overcome the above problems. The monolith-based columns have been commercially available for various types of chromatography since 1990s.

Polymer monoliths from hydrophilic polymers such as chitosan and poly(γ-glutamic acid) (PGA), are especially suitable for bio-applications including tissue engineering, biomolecules immobilization, and drug delivery. Tissue engineering is an important bio-technique to understand the mechanism of tissue growth and provide replacement tissue for the clinical use. The monoliths are useful for tissue engineering because it could provide the pores for the storage of cells and nutrients [3-4]. Moreover, biocompatible and biodegradable monoliths are useful for *in vivo* tissue growth [5]. Polymer

monoliths were applied for the immobilization of biomolecules including enzyme, proteins, and DNA after activating the functional groups of the monoliths [6-7]. In some researches, the enzyme immobilized monoliths were further applied as bioreactors (in bath or flow-through type) [8-9]. Moreover, the efficiency of the polymer monoliths for the controlled drug delivery was reported [10].

Another important application of polymer monoliths is the carrying of catalyst. In this system, the monoliths provide continuous pores for enhanced mass transfer of molecules and the attached catalysts provide active catalytic sites. An example is the Suzuki-Miyaura cross-coupling (SMC) reaction catalyzed by the palladium-loaded poly(acrylonitrile) monoliths [11]. By controlling the surface of polymer monoliths, the affinity of the catalyst toward the monoliths could be increased, which is crucial to get a catalyst with low leaching property and high reusability [12].

Some other applications of polymer monoliths are waste water treatment [13] and ion exchange [14]. In both cases, the advantage of the monoliths over other types of polymer materials is that the monoliths could enable the flow-through of the solutions.

Another popular type of monoliths is carbon monolith which has been widely used as electrode for battery or supercapacitor. The performance of the electrode is predominantly determined by the electrode surface area. Thus, carbon monoliths of high surface area have been widely developed [15]. To fulfill different applications, the sulfur or nitrogen-doped carbon monoliths were also researched [16-17]. Other applications of carbon monoliths include oil-water separation [18], catalyst carrier [19], and carbon dioxide adsorption[20].

Silica monoliths are the most well-known inorganic monoliths, showing great potential to be used as separation columns for the chromatography. In this application, the considerable shrinkage of silica during the polycondensation or heat treatment process has

been overcome by Tanaka in 1990s. After that, various silica monolith-based columns were developed and commercial availably in 2000s. In some other applications, silica monoliths are used as matrixes for the carrying of catalyst or the enzyme immobilization [21-22]. However, the silica monoliths are inferior in these applications because the modification of silica is not as easy as that of the polymer monoliths.

Table 1. Various types of monoliths and their applications.

Types of monoliths	Applications
Polymer monoliths	Catalyst [32] Ion exchange [14] Drug delivery [10] Waste water treatment [13] Separation media [24] Tissue engineering [33] Enzyme immobilization [9,34-35]
Silica monoliths	Catalyst [36] Separation media [37] Enzyme immobilization [21-22]
Carbon monoliths	Electrode [38-39] Catalyst [19] Oil-water separation [18] Carbon dioxide capture [20]
Ceramic monoliths	Catalyst [40-42]
Metal monoliths	Catalyst [43-44]

The less common popular monoliths are ceramic and metal monoliths, which are corrosion resistant to common organic solvents. Thus, they are mainly used as matrixes for the carrying of catalyst [21-23]. All the monoliths and their applications are summarized as Table 1.

Among all the above mentioned monoliths, the polymer monoliths are easy for modification, showing much more potential applications. Moreover, they could be used as precursors to prepare carbon monoliths, and as templates to prepare silica, ceramic, and metal monoliths. Thus, this thesis will focus on the development of polymer monoliths. As shown in Table 2, various methods have been applied to the synthesis of polymer monoliths from their corresponding monomers including free radical polymerizations, high internal phase emulsion polymerizations, living polymerizations, and polycondensations.

Free radical polymerizations including thermally initiated polymerizations [23], photo initiated polymerizations [24], and radiation polymerizations [25-26], are widely used for the preparation of polymer monoliths. Polymerization of a solution containing monomers, cross-linkers, and porogens in a vessel could give polymer monoliths with porous structure. To fulfil different applications, the pore size distribution of the monoliths could be controlled properly by adjusting the fabrication parameters.

Another widely used method to prepare polymer monoliths is high internal phase emulsion polymerization [27]. In this technique, the synthesis was completed within high internal phase emulsions. The dispersed phase usually is the mixture of water, initiators, and stabilizers. The continuous phase is the mixture of monomers, cross-linkers, and emulsifiers. The dispersed phase could be removed after polymerization, leaving pores connected by skeletons. The contents of dispersed phase can be over 90%, making the final monoliths with high porosity.

Table 2. Different methods to prepare polymer monoliths.

Preparation methods	Examples
Free radical polymerizations	Poly(styrene-*co*-divinylbenzene) monoliths [45] Poly(glycerol dimethacrylate) monoliths [46]
Living polymerizations	Cyclooctene monoliths [5] Poly(divinylbenzene) monoliths [28]
Polycondensations	Urea-formaldehyde resin monoliths [29] Polyglycerol-3-glycidyl ether monoliths [47]
High internal phase emulsion polymerizations	Poly(glycidyl methacrylate-*co*-ethylene dimethacrylate) monoliths [27] Poly(glycidyl methacrylate-*co*-divinylbenzene) monoliths [48]
Thermally-induced phase separation	Poly(acrylonitrile) monoliths [30,49] Polycarbonate monoliths [50-51]

A less common method to synthesize polymer monoliths is living polymerization [28]. It is one kind of chain growth polymerization where the termination ability of a growing polymer chain is missing. By employing living polymerization to monolith synthesis, the degree of polymerization gradually increases in a stepwise way. Thus, the synthesized monoliths show homogenous pore structures.

Polycondensation is a step-growth polymerization technique where all polymer chains could grow in the whole reaction process. It was applied for the polymer monolith synthesis because it is less sensitive to oxygen, thus the complicated de-aeration process is not needed. An example is the synthesis of urea-formaldehyde monolith by

polymerization of an aqueous solution of urea and formaldehyde [29].

By using the above methods, polymer monoliths could be prepared from monomers but not from ready-made polymers. Even though monoliths of natural-based polymers such as chitosan, PGA, or cellulose are highly demanded in many applications, such monoliths cannot be prepared by the above conventional methods. Recently, the author's group developed a thermally-induced phase separation (TIPS) technique [30-31] to prepare polymer monoliths from their corresponding polymers. TIPS is a template-free method by simply dissolving a polymer in a solvent at high temperature and subsequent cooling of the polymer solution. In the cooling process, the phase separation takes place to form porous structure. Until now, various polymer monoliths have been prepared from different polymers. These monoliths including their properties and potential applications are summarized as Table 3.

Poly(ethylene-*co*-vinyl alcohol) (EVOH) is a crystalline copolymer with hydrophilic vinyl alcohol and hydrophobic ethylene segments (Fig. 1). EVOH is high cost in production and cannot be prepared by the direct copolymerization of its corresponding monomers because vinyl alcohol is less stable than acetaldehyde with the energy barrier of 42.7 kJ/mol. Thus, EVOH is industrially prepared by special radical copolymerization of ethylene and vinyl acetate, followed by alkaline hydrolysis.

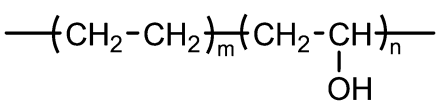

Fig. 1 Chemical structure of EVOH.

EVOH is commercially used in food packing for the beneficial of its excellent gas barrier properties. In addition, EVOH showed other properties such as hydrophilicity, biocompatibility, thermal stability, and chemical resistance. Based on the properties, EVOH has been widely researched in academic for other applications, which are summarized as Table 4.

Table 3. Properties and possible applications of polymer monoliths fabricated through phase separation method.

Polymers	Properties	Possible applications
Acrylic resin	Chemical modification	Separation matrix
	Solvent resistance	Catalyst matrix
Poly(acrylonitrile)	Heat resistance	Precursor for battery material
	Solvent resistance	Separation matrix
Polyolefin	Heat resistance	Battery separator
	Solvent resistance	Matrix for fuel gas
Silk	Hydrophilic	Biomaterial
	Biocompatibility	Cosmetic
Poly(lactic acid)	Biodegradability	Agriculture material
	Biocompatibility	Biomaterial
Polyurethane	Flexibility	Acoustic material
	Absorbability	Cosmetic
Polycarbonate	Impact resistance	Electronic material
	Heat resistance	Acoustic material
Poly(γ- glutamic acid)	Hydrophilic	Biomaterial
	Biocompatibility	Cosmetic
Poly(vinyl alcohol)	Hydrophilic	Biomaterial
	Solvent resistance	Separation matrix
Cellulose	Hydrophilic	Biomaterial
	Solvent resistance	Catalyst matrix

Even though various types of EVOH have been reported including membranes and fibers, EVOH monoliths have never been reported. Unlike PVA or PGA, EVOH is not soluble in water, although it shows good hydrophilicity. Thus, EVOH monoliths are highly useful for various applications in aqueous media without the need for further cross-linking. However, EVOH monoliths can not be prepared from the corresponding monomers using the conventional methods. Thus, a potential route to the fabrication of EVOH monoliths is TIPS technique using EVOH itself as a precursor. This doctoral thesis reports the synthesis of EVOH monoliths by TIPS and their applications in various fields. This doctoral thesis contains 5 chapters.

Table 4. Applications of EVOH and its derivatives.

Applications	Types	Preparation methods
Antifouling [52]	Membrane	Immersion precipitation
Oil water separation [53]	Membrane	Immersion precipitation
Biofuel cells [54]	Membrane	Solution casting
Proton-conductive membranes [55]	Membrane	Solvent casting
Electrochemical sensing [56-57]	Membrane	Solvent casting
Hair follicle regeneration [58]	Membrane	Solvent casting
Drug delivery [59]	Membrane	Solvent casting
Scaffold [60]	Fiber	Wet-spinning technique
Wound healing [61]	Fiber	Electrospinning

Contents of this thesis

Chapter 1

Mesoporous EVOH monoliths were fabricated by TIPS and the hydroxyl groups were activation by carbonyldiimidazole (CDI). Two kinds of EVOH with different ethylene contents were applied for the fabrication of EVOH monoliths. The resulted EVOH monoliths possessed high specific surface area and uniform mesoporous structure. In addition, the morphology of the EVOH monoliths was controlled by changing the fabrication parameters. Furthermore, the hydroxyl groups of the monoliths have been successfully activated by CDI. EVOH monoliths with hydrophilic segments have large potential over hydrophobic polymeric monoliths for bio-related applications such as tissue engineering, protein purification, drug delivery, and enzyme immobilization.

Chapter 2

A unique method was developed for the generation of the silver nanoparticles (AgNPs) embedded mesoporous monoliths for surface enhanced Raman spectroscopy (SERS) applications. The monoliths with uniformly dispersed AgNPs exhibited both ultrasensitive SERS responses and high Raman signal reproducibility toward 4-mercaptobenzoic acid (MBA). Compared with conventional porous SERS substrates, which need complicated fabrication process, the proposed method enabled facile one-pot fabrication of the porous material. We believe that the present porous SERS substrate has great potential for *in situ* chemical or biological studies.

Chapter 3

A new and simple method was developed for fabricating palladium nanoparticles (PdNPs) captured in EVOH monoliths based on TIPS method. XRD result confirmed the

formation of PdNPs inside the monoliths. TEM image showed that most of the captured PdNPs were in the diameter range from 5 nm to 10 nm. The monoliths had relatively high specific surface area and uniform mesoporous structure. To measure its catalytic efficiency, the cross-linked monoliths were applied to a heterogeneous Suzuki-Miyaura reaction of aryl halide and aryl boronic acid in a water/ethanol mixture. The monoliths exhibited both high catalytic performance and excellent stability for repeated use.

Chapter 4

Catalase was immobilized onto the CDI activated EVOH monoliths. The effects of pH and temperature on the activity of free and immobilized catalase were investigated by measuring the efficiency of them for the decomposition of hydrogen peroxide. Furthermore, the thermal stability and reusability of the immobilized catalase were discussed.

Chapter 5

EVOH/chitosan blend monoliths with uniform mesoporous structure and relatively high specific surface area were fabricated by TIPS method. The blend monoliths had three-dimensional interconnected pores and chitosan was found to be lain on the inner surface of the blend monoliths. In addition, the adsorption ability of the blend monoliths toward various kinds of heavy metal ions was studied in a batch adsorption system. The monoliths also showed quick copper ions desorption ability by simply immersing the monoliths into acid solution. By utilizing the unique properties of chitosan, the blend monoliths are expected to have various applications in such as waste water treatment and enzyme immobilization.

References

1. Mould, D.; Synge, R., *Analyst*, **77**, 964-969 (1952).
2. Svec, F.; Fréchet, J. M., *Analytical Chemistry*, **64**, 820-822 (1992).
3. Sušec, M.; Liska, R.; Russmüller, G.; Kotek, J.; Krajnc, P., *Macromolecular Bioscience*, **15**, 253-261 (2015).
4. Christenson, E. M.; Soofi, W.; Holm, J. L.; Cameron, N. R.; Mikos, A. G., *Biomacromolecules*, **8**, 3806-3814 (2007).
5. Bandari, R.; Prager-Duschke, A.; Kühnel, C.; Decker, U.; Schlemmer, B.; Buchmeiser, M. R., *Macromolecules*, **39**, 5222-5229 (2006).
6. Hong, T.; Chi, C.; Ji, Y., *Journal of Separation Science*, **37**, 3377-3383 (2014).
7. Krenkova, J.; Szekrenyes, A.; Keresztessy, Z.; Foret, F.; Guttman, A., *Journal of Chromatography A*, **1322**, 54-61 (2013).
8. Urban, J.; Svec, F.; Fréchet, J. M., *Biotechnology and Bioengineering*, **109**, 371-380 (2012).
9. Lv, Y.; Lin, Z.; Tan, T.; Svec, F., *Biotechnology and Bioengineering*, **111**, 50-58 (2014).
10. Gander, B.; Beltrami, V.; Gurny, R.; Doelker, E., *International Journal of Pharmaceutics*, **58**, 63-71 (1990).
11. Kundu, D.; Patra, A. K.; Sakamoto, J.; Uyama, H., *Reactive and Functional Polymers*, **79**, 8-13 (2014).
12. Bandari, R.; Buchmeiser, M. R., *Catalysis Science and Technology*, **2**, 220-226 (2012).
13. Han, J.; Du, Z.; Zou, W.; Li, H.; Zhang, C., *Journal of Hazardous Materials*, **276**, 225-231 (2014).
14. Eder, K.; Huber, C. G.; Buchmeiser, M. R., *Macromolecular Rapid Communications*,

28, 2029-2032 (2007).

15. Goodman, P. A.; Li, H.; Gao, Y.; Lu, Y. F.; Stenger-Smith, J. D.; Redepenning, J., *Carbon*, **55**, 291-298 (2013).
16. Hasegawa, G.; Aoki, M.; Kanamori, K.; Nakanishi, K.; Hanada, T.; Tadanaga, K., *Journal of Materials Chemistry*, **21**, 2060-2063 (2011).
17. Roberts, A. D.; Wang, S.; Li, X.; Zhang, H., *Journal of Materials Chemistry A*, **2**, 17787-17796 (2014).
18. Qiu, S.; Jiang, B.; Zheng, X.; Zheng, J.; Zhu, C.; Wu, M., *Carbon*, **84**, 551-559 (2015).
19. Ma, X.; Zou, B.; Cao, M.; Chen, S. L.; Hu, C., *Journal of Materials Chemistry A*, **2**, 18360-18366 (2014).
20. Ma, X.; Li, Y.; Cao, M.; Hu, C., *Journal of Materials Chemistry A*, **2**, 4819-4826 (2014).
21. Dubinsky, S.; Petukhova, A.; Gourevich, I.; Kumacheva, E., *Chemical Communications*, **46**, 2578-2580 (2010).
22. Wang, H.; Jiang, Y.; Zhou, L.; He, Y.; Gao, J., *Journal of Molecular Catalysis B: Enzymatic*, **96**, 1-5 (2013).
23. Wang, Q. C.; Švec, F.; Fréchet, J. M., *Journal of Chromatography A*, **669**, 230-235 (1994).
24. Liu, Z.; Ou, J.; Lin, H.; Wang, H.; Dong, J.; Zou, H., *Analytical Chemistry*, **86**, 12334-12340 (2014).
25. Viklund, C.; Irgum, K., *Macromolecules*, **33**, 2539-2544 (2000).
26. Gu, B.; Li, Y.; Lee, M. L., *Analytical Chemistry*, **79**, 5848-5855 (2007).
27. Yao, C.; Qi, L.; Jia, H.; Xin, P.; Yang, G.; Chen, Y., *Journal of Materials Chemistry*, **19**, 767-772 (2009).

28. Kanamori, K.; Nakanishi, K.; Hanada, T., *Advanced Materials*, **18**, 2407-2411 (2006).
29. Sun, X.; Chai, Z., *Journal of Chromatography A*, **943**, 209-218 (2002).
30. Okada, K.; Nandi, M.; Maruyama, J.; Oka, T.; Tsujimoto, T.; Kondoh, K.; Uyama, H., *Chemical Communications*, **47**, 7422-7424 (2011).
31. Nandi, M.; Okada, K.; Uyama, H., *Functional Materials Letters*, **4**, 407-410 (2011).
32. Taori, V. P.; Bandari, R.; Buchmeiser, M. R., *Chemistry - A European Journal*, **20**, 3292-3296 (2014).
33. Park, S. B.; Hasegawa, U.; Van Der Vlies, A. J.; Sung, M. H.; Uyama, H., *Journal of Biomaterials Science, Polymer Edition*, **25**, 1875-1890 (2014).
34. Li, N.; Zheng, W.; Shen, Y.; Qi, L.; Li, Y.; Qiao, J.; Wang, F.; Chen, Y., *Journal of Separation Science*, **37**, 3411-3417 (2014).
35. Han, W.; Yamauchi, M.; Hasegawa, U.; Noda, M.; Fukui, K.; van der Vlies, A. J.; Uchiyama, S.; Uyama, H., *Journal of Bioscience and Bioengineering*, **119**, 505-510 (2015).
36. Song, G. Q.; Lu, Y. X.; Zhang, Q.; Wang, F.; Ma, X. K.; Huang, X. F.; Zhang, Z. H., *RSC Advances*, **4**, 30221-30224 (2014).
37. Azzouz, I.; Essoussi, A.; Fleury, J.; Haudebourg, R.; Thiebaut, D.; Vial, J., *Journal of Chromatography A*, **1383**, 127-133 (2015).
38. Hu, W.; Zhang, H.; Zhang, Y.; Wang, M.; Qu, C.; Yi, J., *Chemical Communications*, **51**, 1085-1088 (2015).
39. Hu, Y. S.; Adelhelm, P.; Smarsly, B. M.; Hore, S.; Antonietti, M.; Maier, J., *Advanced Functional Materials*, **17**, 1873-1878 (2007).
40. Zheng, J.; Salamon, D.; Lefferts, L.; Wessling, M.; Winnubst, L., *Microporous and Mesoporous Materials*, **134**, 216-219 (2010).

41. Ayastuy, J. L.; Gamboa, N. K.; González-Marcos, M. P.; Gutiérrez-Ortiz, M. A., *Chemical Engineering Journal*, **171**, 224-231 (2011).

42. Klein, T. Y.; Treccani, L.; Thöming, J.; Rezwan, K., *RSC Advances*, **3**, 13381-13389 (2013).

43. Bagge-Hansen, M.; Wichmann, A.; Wittstock, A.; Lee, J. R. I.; Ye, J.; Willey, T. M.; Kuntz, J. D.; Van Buuren, T.; Biener, J.; Bäumer, M.; Biener, M. M., *Journal of Physical Chemistry C*, **118**, 4078-4084 (2014).

44. Guo, Q.; Zhao, Y.; Liu, J.; Ma, C.; Zhou, H.; Chen, L.; Huang, B.; Wei, W., *Journal of Materials Chemistry A*, **3**, 10179-10182 (2015).

45. Hird, N.; Hughes, I.; Hunter, D.; Morrison, M. G. J. T.; Sherrington, D. C.; Stevenson, L., *Tetrahedron*, **55**, 9575-9584 (1999).

46. Aoki, H.; Kubo, T.; Ikegami, T.; Tanaka, N.; Hosoya, K.; Tokuda, D.; Ishizuka, N., *Journal of Chromatography A*, **1119**, 66-79 (2006).

47. Peskoller, C.; Niessner, R.; Seidel, M., *Journal of Chromatography A*, **1216**, 3794-3801 (2009).

48. Barbetta, A.; Dentini, M.; Leandri, L.; Ferraris, G.; Coletta, A.; Bernabei, M., *Reactive and Functional Polymers*, **69**, 724-736 (2009).

49. Nandi, M.; Okada, K.; Uyama, H., *Functional Materials Letters*, **4**, 407-410 (2011).

50. Xin, Y.; Fujimoto, T.; Uyama, H., *Polymer (United Kingdom)*, **53**, 2847-2853 (2012).

51. Xin, Y.; Uyama, H., *Chemistry Letters*, **41**, 1509-1511 (2012).

52. Miao, R.; Wang, L.; Gao, Z.; Mi, N.; Liu, T.; Lv, Y.; Wang, X., *RSC Advances*, **5**, 36325-36333 (2015).

53. Bai, Y.; Liang, L.; Zhang, C.; Gu, J.; Sun, Y., *Shiyou Huagong/Petrochemical Technology*, **40**, 1247-1252 (2011).

54. Chen, W. J.; Lee, M. H.; Thomas, J. L.; Lu, P. H.; Li, M. H.; Lin, H. Y., *ACS Applied*

Materials and Interfaces, **5**, 11123-11128 (2013).

55. Chiba, Y.; Tominaga, Y., *Journal of Power Sources*, **203**, 42-47 (2012).
56. Chung, I. C.; Chang, C. C.; Chiu, H. S.; Jiang, S. F.; Lee, M. H.; Chung, C. L.; Liu, B. D.; Huang, C. Y.; Lin, H. Y., *Journal of Nanoscience and Nanotechnology*, **11**, 10633-10638 (2011).
57. Huang, C. Y.; O'Hare, D.; Chao, I. J.; Wei, H. W.; Liang, Y. F.; Liu, B. D.; Lee, M. H.; Lin, H. Y., *Biosensors and Bioelectronics*, (2014).
58. Young, T. H.; Lee, C. Y.; Chiu, H. C.; Hsu, C. J.; Lin, S. J., *Biomaterials*, **29**, 3521-3530 (2008).
59. Lai, P. S.; Young, T. H.; Wang, C. Y.; Shieh, M. J., *Biomedical Engineering - Applications, Basis and Communications*, **17**, 86-90 (2005).
60. Susano, M. A.; Leonor, I. B.; Reis, R. L.; Azevedo, H. S., *Journal of Applied Polymer Science*, **131,** (2014).
61. Wang, B.; Xu, C.; Xu, F.; Lu, T., *Journal of Nanomaterials*, **2011,** (2011).

Chapter 1

Reactive poly(ethylene-*co*-vinyl alcohol) monoliths with tunable pore morphology

1.1 Introduction

Mesoporous materials with the structural capabilities at the scale of a few nanometers and large surface area can meet the demands of growing applications such as protein immobilization, adsorption, ion-exchange, catalysis, sensors, etc. Fabrication of mesoporous materials based on inorganic or organic-inorganic hybrid frameworks has been widely adopted using organic molecules as templates [1-4]. However, little research has been done on purely organic mesoporous materials by similar methods; such trials often lead to collapse of the mesopore structure during template removal process [5-6]. Thus, fabrication of mesoporous polymer materials with a template-free method is a challenge work.

As described in the general introduction section, EVOH is a crystalline copolymer with hydrophilic vinyl alcohol and hydrophobic ethylene segments [7]. EVOH has drawn much attention as a unique biomedical material because EVOH has many advantages such as hydrophilicity, biocompatibility, thermal stability, and chemical resistance. Unlike PVA or PGA, EVOH is not soluble in water, although it shows good hydrophilicity. Thus, EVOH monoliths are highly useful for various applications in aqueous media without the need for further cross-linking.

In this chapter, mesoporous EVOH monoliths were fabricated by TIPS and their hydroxyl groups were activation by carbonyldiimidazole (CDI). Two kinds of EVOH with different ethylene contents were applied for the fabrication of EVOH monoliths. The

morphology of the EVOH monoliths was controlled by changing the fabrication parameters. Additionally, the hydroxyl groups of the monoliths were successfully activated by CDI.

1.2 Experimental

Materials

Two kinds of EVOH with ethylene content of 27 and 44 mol% (abbreviated as EVOH 27 and EVOH 44, respectively), were supplied from Sigma Co. CDI, isopropanol (IPA), acetone and acetonitrile (ACN) were purchased from Wako Co. All reagents were used as received without further purification.

Fabrication of EVOH monolith

The general procedure for the fabrication of an EVOH monolith is illustrated in Fig. 1-1. For the fabrication of an EVOH 27 monolith from an EVOH 27 solution (140 mg/mL), the experiment process is as follows. An EVOH 27 solution was prepared by dissolving 140 mg of EVOH 27 in a mixture of 0.65 mL of IPA and 0.35 mL of water at 75 ^{o}C and the solution was cooled at 20 ^{o}C. During the cooling stage, the phase separation took place to form the monolith, which was immersed into a large amount of acetone to remove the embedded solvent and subsequently dried under vacuum.

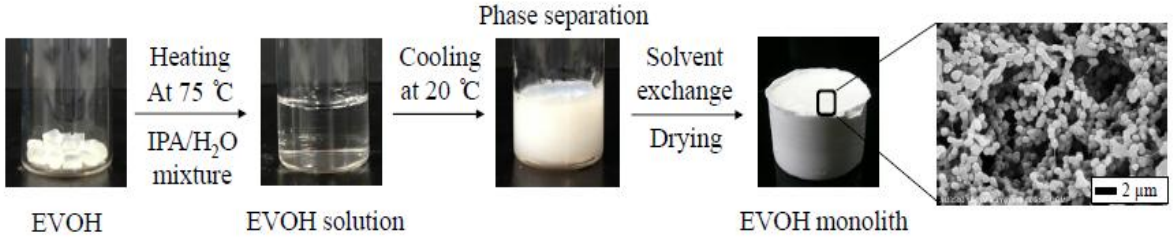

Fig. 1-1 Fabrication procedure of EVOH monolith

Characterization

Scanning electron microscope (Hitachi Co., SU3500) was used to observe the

monolith cross sections. Before the measurement, the monolith was fractured to small pieces, mounted on a SEM stub, and sputtered with pure gold in vacuo. SEM images were recorded at an accelerating voltage of 15 kV. Nitrogen adsorption/desorption isotherms for the EVOH monolith were measured with a NOVA-4200e surface area & pore size analyzer (Quantachrome Instruments) at 77 K. The multi-point Brunauer Emmett Teller (BET) method and non-local density functional theory (NLDFT) method were used to determine the specific surface area and the pore size distribution plot, respectively. Fourier transform infrared (FT-IR) measurements were performed with Thermo Scientific (Yokohama, Japan) Nicolet iS5 by the attenuated total reflectance method. Elemental analysis was carried out on a CHN corder MT-5 (Yanaco New Science Inc.). UV was measured by an Infinite 200 (Tecan) microplate reader.

Activation of EVOH monolith

EVOH monolith (0.1 g) was immersed in 5 mL of ACN solution containing CDI (0.2 g). The reaction was carried out at 40 ^{o}C for 4 h. Afterwards, the monolith was washed thoroughly with acetone and subsequently dried under vacuum. The resulting CDI-modified EVOH monolith (CDI-EVOH monolith) was stored in 4 ^{o}C for further uses.

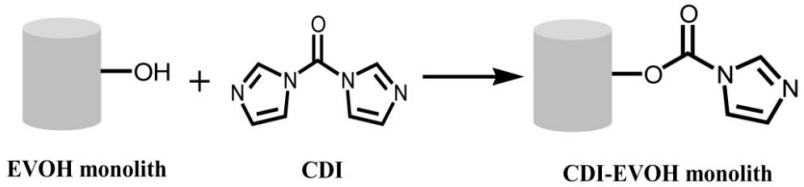

Scheme 1-1 Modification of EVOH monolith.

1.3 Results and discussion

Fabrication and characterization of EVOH monolith

Generally, a mediate affinity of polymers toward solvent molecules is a key factor to fabricate monolith by TIPS method. EVOH is insoluble in neither IPA nor water. Interestingly, EVOH 27 became soluble in a mixture of IPA and water (65:35 vol%) at 75

^{o}C. The EVOH solution with the concentration of 140 mg/mL in this mixed solvent was kept at 20 ^{o}C. During the cooling course, the phase separation took place to form the monolith (Fig. 1-1). This unique behavior is probably based on cosolvency effect [8-9]; a poly(methyl methacrylate) monolith was prepared on the basis of the cosolvency by using a mixture of ethanol and water as phase separation solvent [8].

The inside morphology of the EVOH monolith was observed by SEM, which shows the three-dimensional open pore structure of the monolith (Fig. 1-1). The average pore and skeleton sizes of the monolith were 2.9 μm and 1.9 μm, respectively. The nitrogen adsorption/desorption isotherms for the monolith indicate the formation of mesoporous structure. By using the non-local density functional theory (NLDFT) method, the pore size distribution (PSD) plot for the EVOH monolith was obtained, which reveals uniform pores with diameter of ca. 5.0 nm. The specific surface area was measured as 93.1 m^2 g^{-1} by multi-point BET method. These data indicate the formation of relatively uniform mesopores and macropores in the EVOH monolith.

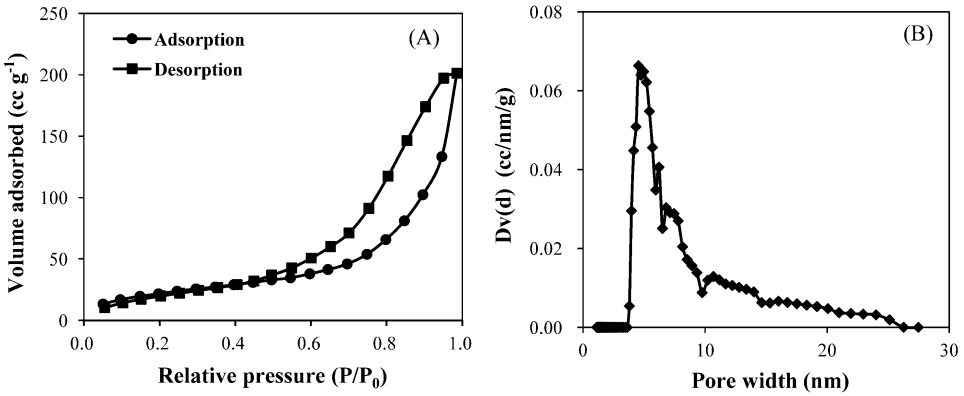

Fig. 1-2 Nitrogen adsorption-desorption isotherm of the EVOH 27 monolith (A) and pore size distribution of the monolith by NLDFT method (B).

By changing the polymer concentration and the composition of the mixed solvent, the range of the monolith formation was examined. When the water ratio in the mixed solvent was 35 %, the monolith was formed in the polymer concentration from 80 to 180

mg/mL. In case of the polymer concentration of 100 mg/mL, the formation of the monolith with bicontinuous structure was observed in the water ratio was 30, 35, or 55 %, whereas the polymer was soluble even at room temperature in the range of the water ratio from 40 to 50 %. In the higher polymer concentration (150 mg/mL), the monolith was formed in the range of the water ratio from 35 to 55 %. These data clearly show the strong dependence of the monolith formation on the polymer concentration and solvent composition. The effect of the polymer concentration may be explained as follows. The lower concentration may result in insufficient numbers of the EVOH chains to form the continuous skeleton structure and the phase separation is difficult to occur because of higher viscosity in case of the higher concentration.

EVOH 44 was also available for the monolith fabrication under the similar conditions. When the concentration of EVOH 44 was in the range from 140 to 200 mg/mL, the monolith with the bicontinuous structure was obtained, which range was smaller than that for EVOH 27. In case of the concentration less than 120 mg/mL, the monolith formation was not observed. This may be due to the difference of the hydrophilicity of EVOH.

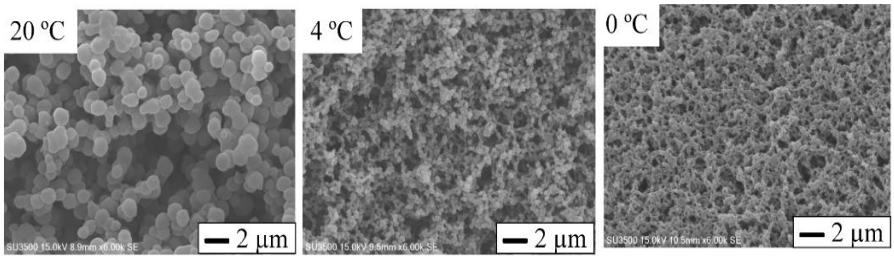

Fig. 1-3 SEM images of EVOH 27 monoliths at different cooling temperatures (polymer concentration: 140 mg/mL).

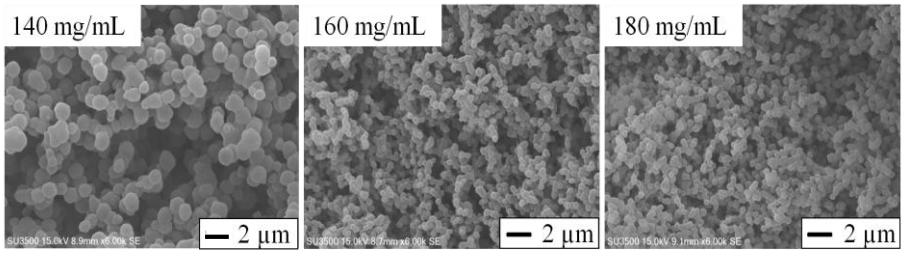

Fig. 1-4 SEM images of EVOH 27 monoliths at different polymer concentrations (cooling temperature: 20 ^{o}C).

Morphology control of EVOH monolith

Effects of various fabrication parameters on the morphology of the EVOH monolith have been systematically investigated. The effect of the cooling temperature on the morphology of the EVOH monolith is shown in Fig. 1-5. When the cooling temperature changed from 20 °C to 0 °C, the average pore size of the monolith decreased from 2.9 μm to 0.5 μm and the skeleton size decreased from 1.9 μm to 0.4 μm (Fig. 1-3 and Fig. 1-5(A)) for EVOH 27. This may be because at higher cooling temperature, the phase separation process takes place more slowly, leading to the formation of large pores

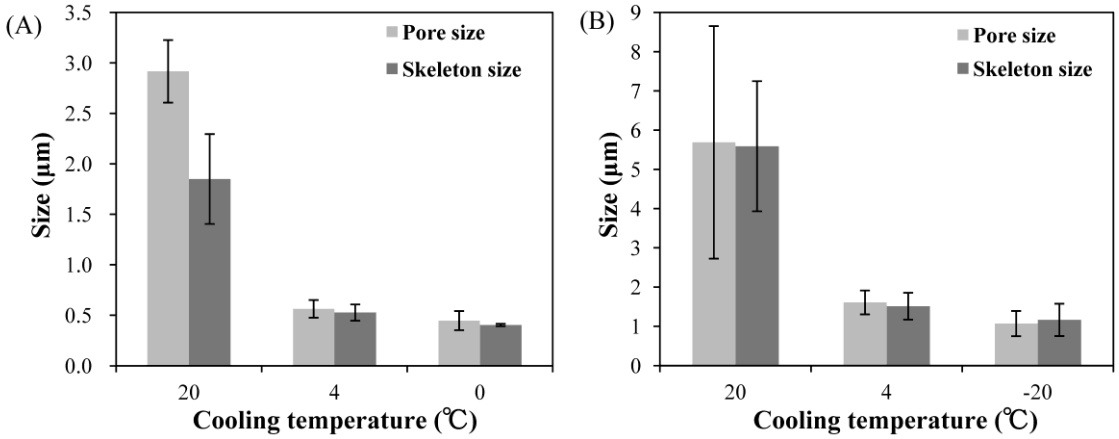

Fig. 1-5 Effect of cooling temperature on average pore and skeleton sizes of EVOH 27 (A) and EVOH 44 (B) monoliths (polymer concentration: 140 mg/mL).

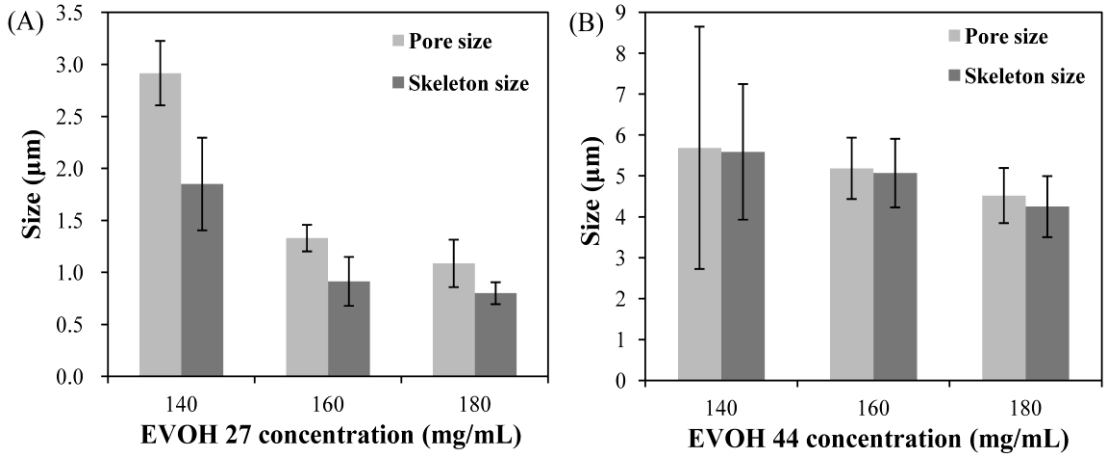

Fig. 1-6 Effect of polymer concentration on average pore and skeleton sizes of EVOH 27 (A) and EVOH 44 (B) monoliths (cooling temperature: 20 °C).

[10]. As for EVOH 44, the pore and skeleton sizes of the monolith were larger than those for EVOH 27, probably due to the different affinity and/or solubility of the polymer toward the phase separation solvent. In all cases examined, the relatively uniform structure was observed. These dates suggest that the pore and skeleton sizes could be controlled by changing the cooling temperature.

The polymer concentration also affected on the morphology of the EVOH monolith. As the concentration increased from 140 mg/mL to 180 mg/mL, the average pore sizes decreased from 2.9 μm to 1.1 μm and the skeleton sizes decreased from 1.9 μm to 0.8 μm (Fig. 1-4 and Fig. 1-6 (A)) for EVOH 27. This could also be explained by the relationship of viscosity and phase separation. At higher polymer concentration, the phase separation process occurs more quickly in the viscous polymer solution, resulting in the formation of smaller skeleton pores. For EVOH 44, the similar behavior of the monolith formation was observed and the change of the pore and skeleton sizes against the polymer concentration was smaller than that for EVOH 27 (Fig. 1-6 (B)).

Activation of EVOH monolith

CDI is a well-known reagent to activate a hydroxyl group for introduction of functional molecules [11-12]. As shown in Scheme 1-1, the hydroxyl group of EVOH on the monolith surface was modified by CDI for introduction of urease on the monolith. Fig. 1-7 shows the FT-IR spectra of EVOH and CDI-EVOH monolith. A broad peak at 3325 cm^{-1} due to the

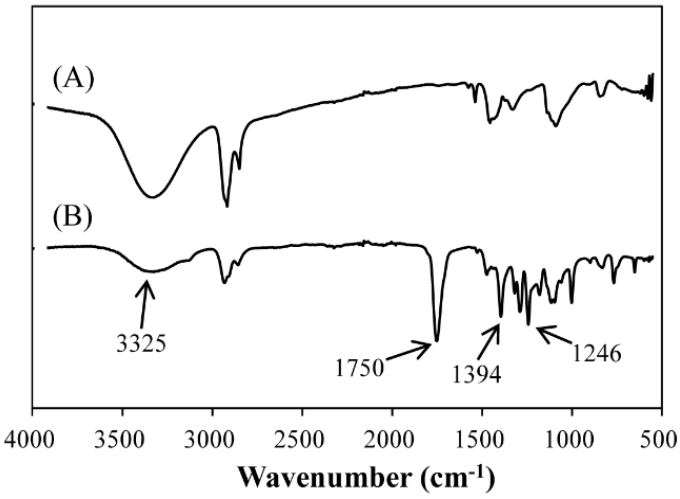

Fig. 1-7 FT-IR spectra of EVOH 27 monolith (A) and CDI-modified EVOH 27 monolith (B).

hydroxyl group decreased after the activation by CDI. The imidazolyl-carbamate group of the product was confirmed by a peak at 1750 cm^{-1} due to asymmetric stretch of the carbonyl group, a peak at 1460 cm^{-1} to CH_2 scissor of deformation of CDI, peaks at 1394 cm^{-1} and 1246 cm^{-1} to C-N stretches of CDI. These data show the successful modification of EVOH monolith by CDI.

The modification by CDI would be mainly made on the monolith surface. As a measure of the modification monitoring, the elemental analysis of the CDI-EVOH monolith was carried out (Fig. 1-8). The nitrogen content in the monolith increased with increasing the CDI concentration, suggesting the control of the surface composition as a function of the CDI concentration.

The mechanical strength of the CDI-EVOH monolith prepared by using 60 and 80 mg/mL CDI was found to be inferior to that by the lower concentration of CDI or of the unmodified monolith by qualitative evaluation. Thus, the monolith modified by using 40 mg/mL CDI, which possessed relatively good toughness and high content of the activated group, was used for further applications.

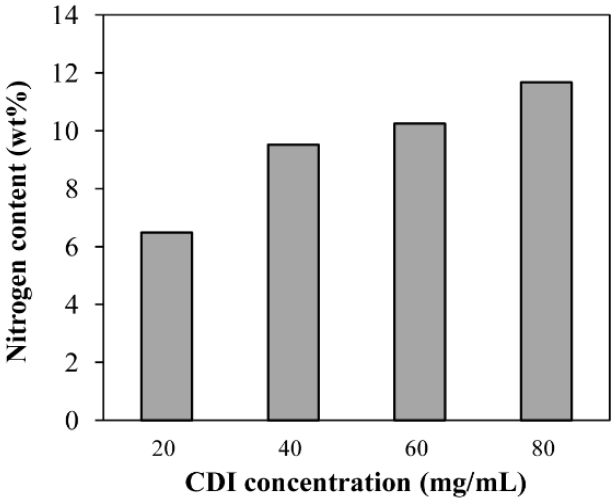

Fig. 1-8 Elemental analysis results of CDI-modified EVOH 27 monolith.

1.4 Conclusions

A mesoporous EVOH monolith was fabricated from the EVOH solution in a mixed solvent of IPA and water by TIPS. The morphology of the monolith could be controlled by altering the fabrication conditions such as the mixed ratio of IPA and water,

the cooling temperature and the concentration of EVOH. The resulting EVOH monolith possessed large specific surface area and uniform mesoporous structure. Moreover, the hydroxyl groups of the monolith were successfully activated by CDI.

Unlike PVA, EVOH is insoluble in water, although it shows high hydrophilicity. Thus, the cross-linking is not required for usage of the EVOH monolith in aqueous media. Additionally, nonionic and hydrophilic EVOH is a suitable material for suppression of non-specific adsorption of biomolecules such as proteins and DNA. Based on these characteristics, the present EVOH monolith may be useful for a variety of bio-related applications.

1.5 References

1. Wan, Y.; Zhao, D., *Chemical Reviews*, 107, 2821-2860 (2007).
2. Li, W.; Zhao, D., *Chemical Communications*, 49, 943-946 (2013).
3. Kresge, C. T.; Leonowicz, M. E.; Roth, W. J.; Vartuli, J. C.; Beck, J. S., *Nature*, 359, 710-712 (1992).
4. Langley, P. J.; Hulliger, J., *Chemical Society Reviews*, 28, 279-291 (1999).
5. Chandra, D.; Jena, B. K.; Raj, C. R.; Bhaumik, A., *Chemistry of Materials*, 19, 6290-6296 (2007).
6. Modak, A.; Mondal, J.; Sasidharan, M.; Bhaumik, A., *Green Chemistry*, 13, 1317-1331 (2011).
7. Lv, R.; Zhou, J.; Du, Q.; Wang, H.; Zhong, W., *Journal of Membrane Science*, 281, 700-706 (2006).
8. Yoneda, S.; Han, W.; Hasegawa, U.; Uyama, H., *Polymer (United Kingdom)*, 55, 3212-3216 (2014).
9. González-Benito, J.; Koenig, J. L., *Polymer*, 47, 3065-3072 (2006).
10. Xin, Y.; Fujimoto, T.; Uyama, H., *Polymer (United Kingdom)*, 53, 2847-2853 (2012).
11. Bethell, G. S.; Ayers, J. S.; Hancock, W. S.; Hearn, M. T., *Journal of Biological Chemistry*, 254, 2572-2574 (1979).
12. Li, Y. C.; Liao, Y. T.; Chang, H. H.; Young, T. H., *Colloids and Surfaces B: Biointerfaces*, 102, 53-62 (2013).

Chapter 2

Mesoporous poly(ethylene-*co*-vinyl alcohol) monoliths captured with silver nanoparticles as SERS substrates: facile fabrication and ultra-high sensitivity

2.1 Introduction

Surface-enhanced Raman spectroscopy (SERS) has attracted the interest of scientists as a powerful technique to detect chemical and biological molecules of trace concentration. The ultra-high sensitivity is due to the enhancement of local electromagnetic field caused by nano-scale gaps (also called Raman "hot spots") between metal nanostructures. Metal nanoparticles or nanostructures in the types of roughed metal electrodes [1-3], metal nanoparticles colloids [4-6], metal nanoparticles-assembled planar substrates [7-8], and metal nanoparticles-embedded three-dimensional (3-D) porous substrates [9] have been developed as efficient SERS substrates. Among these SERS substrates, the 3-D porous ones are preferred because the open pores and the high surface area enable fast permeation and efficient adsorption of target analytes, respectively. In addition, porous structure is considered to be able to improve the SERS performance in a large scale [10].

So far, various 3-D porous SERS substrates have been prepared by immobilizing metal nanoparticles into a porous matrix such as porous gel [10], nanofiber [11], porous alumina [9], porous silicon [12], monolith [13-14], MOF [15] and paper [16]. For the construction of SERS substrates, a facile, cost-effective and largely-scalable method is highly demanded. However, the preparation of metal nanoparticles and a porous matrix is generally in

separated processes, which is costly and somewhat wearisome. Thus, it remains a great challenge for preparation of 3-D porous SERS substrates by a simply one-pot process.

Mesoporous polymer monoliths with open pores and large surface areas are especially useful for applications of 3-D porous SERS substrates. In order to get monolith-based 3-D SERS substrates with uniform mesopores, well dispersed metal nanoparticles and high SERS signal reproducibility, facile synthesis of a metal-polymer monolith using a one-pot process is indispensable and of particular interest.

In this chapter, a new and straightforward method to embed AgNPs into a mesoporous EVOH monolith (AgNPs-EVOH monolith) was developed. The monolith was further used as a SERS substrate with both ultrasensitive SERS responses and high SERS signal reproducibility. This study enables the preparation of a 3-D porous SERS substrate with a facile method, which is as simple as other methods [17-18].

2.2 Experimental

Materials

Poly(ethylene-*co*-vinyl alcohol) (EVOH) with ethylene content of 27 mol % was supplied from Sigma. The number average molecular weight and weight average molecular weight measured by SEC were 6.8×10^4 and 1.6×10^5, respectively. 4-Mercaptobenzoic acid (MBA), rhodamine 6G (R6G), ethanol, isopropanol (IPA), acetone and silver nitrate were purchased from Wako Co. All reagents were used as received without further purification.

Instrumentation

Scanning electron microscope (SEM) observations were carried by using Hitachi Co., SU3500 at an accelerating voltage of 15 kV. Before observations, the monolith was pretreated by sputtering with pure gold in vacuo. The nitrogen adsorption/desorption

isotherms of the AgNPs-EVOH monoliths were measured by using a NOVA-4200e surface area & pore size analyzer (Quantachrome Instruments) at 77 K. Energy dispersive X-ray spectrometric (EDX) result was obtained by utilizing Hitachi Miniscope TM3000 with a Swift 3000 equipment. Transmission electron microcopy (TEM) images of the monolith were recorded in a Hitachi H-7650 TEM.

For Raman imaging, fragments of AgNPs -EVOH monoliths were put onto a glass plate. They were mounted onto the sample stage of Zeiss inverted optical microscope (Axiovert 200), subsequently. A diode-pumped solid-state (DPSS) laser beam (Photop Suwtech, DPGL-2100) with a wavelength of 532 nm was focused using a 10x objective lens onto a monolith fragment. The intensity of laser beam through the objective lens was 2 mW. The Raman spectra were detected by a spectrometer consisting of a polychromator (Andor, SR-303i) and a charge-coupled device (CCD) camera (Andor, DU970P-BV). In order to block the excitation laser beam, a long-pass edge filter (Semlock, LP03-532RU) was placed in the optical path to the spectrometer. Each Raman spectrum was obtained for 10 sec in the spectral range of 100-3700 cm^{-1}.

Preparation of AgNPs-EVOH monoliths

A typical procedure for the preparation of a AgNPs-EVOH monolith was as follows. EVOH (300 mg) was dissolved in a mixed solvent of IPA (1.3 mL) and water (0.7 mL) at 75 ^{o}C to prepare the EVOH solution. Two hundred mg of silver nitrate was added to the solution and stirred for

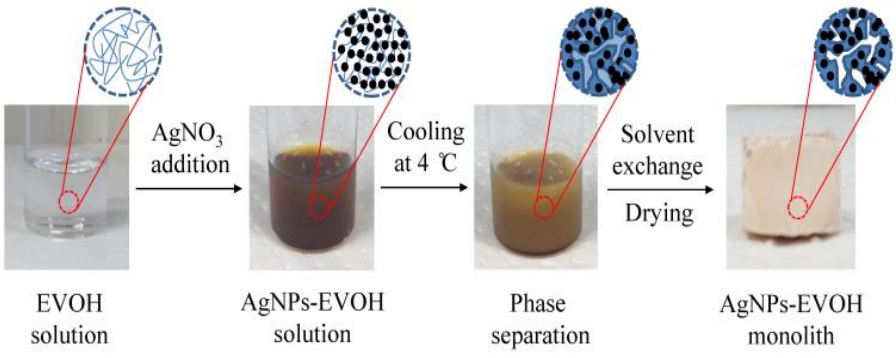

Fig. 2-1 Fabrication procedure of Ag-NPs-EVOH monolith

6 h. Then the solution was cooled at 4 ^{o}C to form the AgNPs-EVOH monolith. The embedded solvents were removed by immersing the monolith into acetone and subsequently the monolith was dried under vacuum.

SERS evaluations

AgNPs-EVOH monolith (20 mg) was immersed in 10 mL of R6G (10^{-6} M) ethanol solution for 2 h. Afterwards, the sample was washed by excessive amount of ethanol to remove unbounded R6G molecules, and the sample was dried in room temperature to remove ethanol. The sample was grinded to mesoporous EVOH powder for further SERS measurements.

In the case of MBA, a stock ethanol solution of MBA with the concentration of 10^{-3} M was prepared. This solution was diluted to give the MBA solutions of the appropriate concentration. AgNPs-EVOH monolith was treated by the solutions using a similar procedure as the case of R6G.

2.3 Results and discussion

The general procedure for the fabrication of the mesoporous AgNPs-EVOH monolith is illustrated in Fig. 2-1. Silver nitrate was added to an EVOH solution of a mixed solvent of isopropanol (IPA) and water (IPA/water: 65/35 (v/v)) at 75 ^{o}C and the solution was gently stirred. The solution was cooled to 4 ^{o}C to form a monolith by TIPS. The resulting monolith was immersed into acetone to remove the embedded solvent and subsequently dried under vacuum. In this method, IPA acted both as a component of the mixed solvent to dissolve EVOH at the high temperature and as an agent for the reduction of the silver ion; the analysis of the solution after the monolith formation suggested that more than 97% of silver ion was reduced. EVOH was initially acted as a stabilizer to protect AgNPs from large scale aggregation and subsequently acted as a gelator to form

the monolith with uniform mesopores. The present simple method to prepare the metal nanoparticles-embedded monolith is suitable for large scale production. Moreover, the monolith could be tailored into any desired shapes for the further SERS applications.

The nitrogen adsorption/desorption isotherms of the monolith exhibited a typical V isotherm with a relatively wide type H1 hysteresis loop in the P/P_0 range from 0.7-0.9, which is the characteristic of the mesoporous structure (Fig. 2-2). The formation of uniform mesopores centred at *ca.* 5.0 nm was proved by the pore size distribution (PSD) plot (insert), which was obtained by using the non-local density functional theory (NLDFT) method. The specific surface area was determined as 60.1 m^2 g^{-1} by multi-point BET method. These data indicate that the AgNPs-EVOH monolith had relative uniform mesopores and large specific surface area.

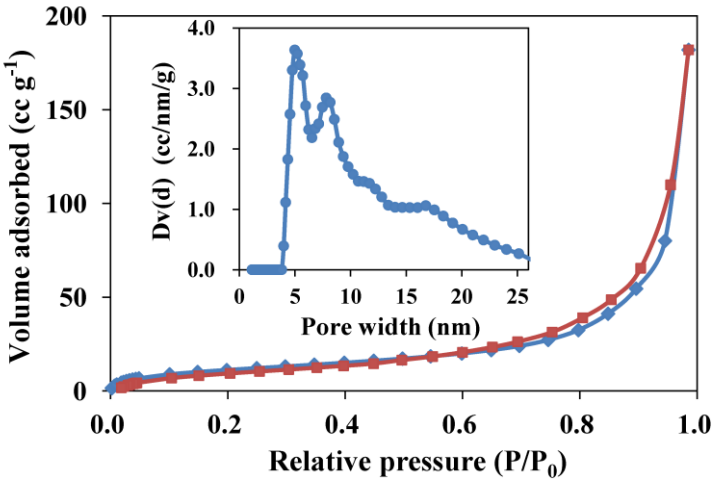

Fig. 2-2 Nitrogen adsorption/desorption isotherms of AgNPs-EVOH monolith. Adsorption points are marked by blue tetragons and desorption points by dark red tetragons.
Inset: Pore size distribution (PSD) using NLDFT model.

Fig. 2-3A shows a scanning electron microscope (SEM) image of the monolith. The SEM image clearly indicates the 3-D open macropore structure of the monolith. The existence of both mesopores and macropores enabled the capture of more target analytes and faster transport of these molecules to the surface of AgNPs. A transmission electron microscopy (TEM) image implies the existence of AgNPs with a typical diameter of 5-20 nm (Fig. 2-3B). It is interesting that most of the formed AgNPs were not spatially-isolated, but partially aggregated as silver dimers or clusters. Many researchers revealed that strong

SERS signals often present at the junction of several nanoparticles [19]. On the other hand, single nanoparticles often result in little enhancement. Thus, the formation of partially aggregated AgNPs made the monolith a potential SERS substrate with ultra sensitivity. The corresponding energy dispersive X-ray spectrometric (EDX) map (Fig. 2-3C) of the monolith shows that the AgNPs were dispersed homogeneously in the 3-D porous monolith, although the EDX mapping was somewhat affected by the rough surface of the monolith. Fig. 2-3D demonstrates the SERS spectrum of rhodamine 6G (R6G) from the monolith that was treated with a R6G solution at concentration of 10^{-6} M. R6G showed characteristic SERS peaks, whereas the monolith exhibited clear background without any significant peaks in the Raman shift range from 900 cm^{-1} to 1900 cm^{-1}. All of these results indicate that the present monolith could be used as a good SERS substrate.

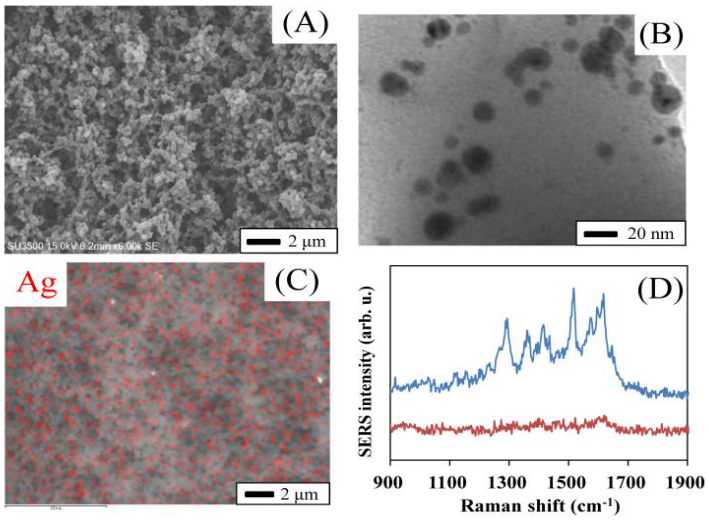

Fig. 2-3 SEM (A), TEM (B) and EDX (C) (red spots represent the existence of AgNPs) images of AgNPs-EVOH monolith. SERS spectrum (—) of R6G collected from the monolith and Raman spectrum (—) of the monolith (without R6G) (D).

To evaluate the efficiency of the AgNPs-EVOH monolith as a SERS substrate, 4-mercaptobenzoic acid (MBA) was selected as a target analyte. We immersed the monolith into 10 mL of ethanol solution containing 10^{-5} M of MBA for 2 h. SERS spectra of MBA collected from 10 randomly selected positions of the monolith are shown in Fig. 2-4. A peak at around 1390 cm^{-1} arose from carboxyl stretching mode and peaks observed at around 1100 cm^{-1} and 1600 cm^{-1} could be attributed to breathing and stretching modes

of aromatic ring, respectively [20]. It should be noted that the SERS responses of the monolith showed good consistency and reproducibility, which is vital in consideration of its practical applications. This may be due to the good dispersion of AgNPs in the monolith.

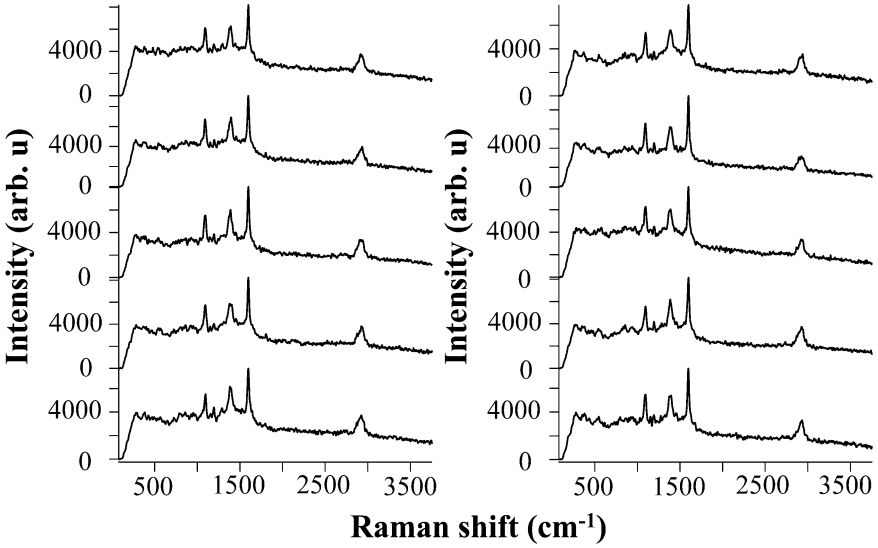

Fig. 2-4 Series of SERS spectra measured in the randomly selected 10 places on the AgNPs-EVOH monoliths.

Several monoliths with different amount of silver nitrate were prepared in order to investigate the influence of the AgNPs concentration. The SEM images (data not shown) clearly show that the monoliths had similar continuous open pores when the weight ratio of silver nitrate/EVOH was equal or lower than 0.67, whereas the monoliths were in non-porous structure in case of the ratio of larger than 0.67. This may be because the IPA/water ratio is changed owing to the consumption of IPA in the Ag^+ reduction process. The SERS spectra of MBA were collected on these samples. Even for the low concentration of MBA (10^{-11} M), the porous monolith showed clear SERS spectra with the same peak positions and similar intensity, whereas no clear spectra were obtained in case of the non-porous monolith. These data indicate that the AgNPs concentration hardly affected the Raman enhancement, while the porous structure was vitally important. Some

researchers also revealed the large effect of porous structure in Raman enhancement [10].

The SERS sensitivity of the monolith toward MBA was investigated by immersing the monolith in the ethanol solution with a wide range of the MBA concentrations from 10^{-3} M to 10^{-13} M. The characteristic Raman peaks of MBA were clear when the MBA concentration was equal or higher than 10^{-7} M (Fig. 2-5). Even the MBA concentration was as low as 10^{-13} M, the peaks at 1100 cm^{-1} and 1600 cm^{-1} were still identifiable, indicating that the present monolith could be applied for ultrasensitive detection of target analytes. Compared with some other SERS substrates, the pesent monolith showed better sensitivity toward MBA [21-22].

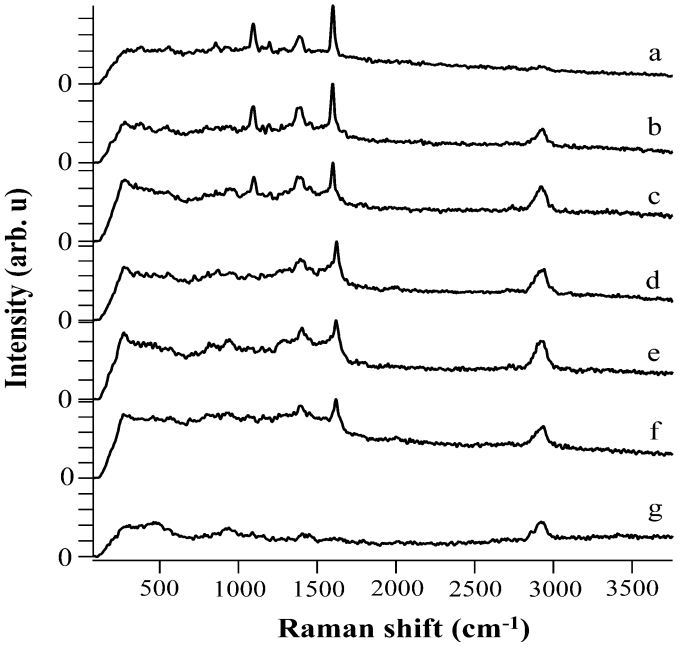

Fig. 2-5 SERS spectrum of MBA on SERS substrate with concentrations of (a) 10^{-3} M, (b) 10^{-5} M, (c) 10^{-7} M, (d) 10^{-9} M, (e) 10^{-11} M, (f) 10^{-13} M, (g) 0 M.

2.4 Conclusion

In this chapter, a unique method was developed for the generation of the AgNPs embedded mesoporous monolith. The monolith with uniformly dispersed AgNPs exhibited both ultrasensitive SERS responses and high Raman signal reproducibility toward MBA. Compared with conventional 3-D porous SERS substrates, which need complicated fabrication process, the proposed method enabled facile one-pot fabrication of the porous material. We believe that the present 3-D porous SERS substrate has great

potential for *in situ* chemical or biological studies.

2.5 References

1. Ren, B.; Lin, X. F.; Yan, J. W.; Mao, B. W.; Tian, Z. Q., *Journal of Physical Chemistry B*, **107**, 899-902 (2003).
2. Gao, P.; Gosztola, D.; Leung, L. W. H.; Weaver, M. J., *Journal of Electroanalytical Chemistry*, **233**, 211-222 (1987).
3. Gao, P.; Weaver, M. J., *Journal of Physical Chemistry*, **89**, 5040-5046 (1985).
4. Zhang, J.; Li, X.; Sun, X.; Li, Y., *Journal of Physical Chemistry B*, **109**, 12544-12548 (2005).
5. Muniz-Miranda, M.; Pagliai, M.; Cardini, G.; Schettino, V., *Journal of Physical Chemistry C*, **112**, 762-767 (2008).
6. Pergolese, B.; Bonifacio, A.; Bigotto, A., *Physical Chemistry Chemical Physics*, **7**, 3610-3613 (2005).
7. Toderas, F.; Baia, M.; Baia, L.; Astilean, S., *Nanotechnology*, **18**(2007).
8. Seitz, O.; Chehimi, M. M.; Cabet-Deliry, E.; Truong, S.; Felidj, N.; Perruchot, C.; Greaves, S. J.; Watts, J. F., *Colloids and Surfaces A: Physicochemical and Engineering Aspects*, **218**, 225-239 (2003).
9. Ko, H.; Chang, S.; Tsukruk, V. V., *ACS Nano*, **3**, 181-188 (2009).
10. Yao, S.; Zhou, C.; Chen, D., *Chemical Communications*, **49**, 6409-6411 (2013).
11. Qian, Y.; Meng, G.; Huang, Q.; Zhu, C.; Huang, Z.; Sun, K.; Chen, B., *Nanoscale*, **6**, 4781-4788 (2014).
12. Virga, A.; Rivolo, P.; Descrovi, E.; Chiolerio, A.; Digregorio, G.; Frascella, F.; Soster, M.; Bussolino, F.; Marchiò, S.; Geobaldo, F.; Giorgis, F., *Journal of Raman Spectroscopy*, **43**, 730-736 (2012).
13. Liu, J.; White, I.; DeVoe, D. L., *Analytical Chemistry*, **83**, 2119-2124 (2011).
14. Guerrouache, M.; Mahouche-Chergui, S.; Chehimi, M. M.; Carbonnier, B., *Chemical*

Communications, **48**, 7486-7488 (2012).

15. Hu, Y.; Liao, J.; Wang, D.; Li, G., *Analytical Chemistry*, **86**, 3955-3963 (2014).
16. Ngo, Y. H.; Li, D.; Simon, G. P.; Garnier, G., *Langmuir*, **28**, 8782-8790 (2012).
17. Lee, A.; Dubinsky, S.; Tumarkin, E.; Moulin, M.; Beharry, A. A.; Kumacheva, E., *Advanced Functional Materials*, **21**, 1959-1969 (2011).
18. Chang, S.; Combs, Z. A.; Gupta, M. K.; Davis, R.; Tsukruk, V. V., *ACS Applied Materials and Interfaces*, **2**, 3333-3339 (2010).
19. Xu, H.; Bjerneld, E. J.; Käll, M.; Börjesson, L., *Physical Review Letters*, **83**, 4357-4360 (1999).
20. Xu, P.; Mack, N. H.; Jeon, S. H.; Doom, S. K.; Han, X.; Wang, H. L., *Langmuir*, **26**, 8882-8886 (2010).
21. Amarjargal, A.; Tijing, L. D.; Shon, H. K.; Park, C. H.; Kim, C. S., *Applied Surface Science*, **308**, 396-401 (2014).
22. Zhu, S.; Fan, C.; Wang, J.; He, J.; Liang, E.; Chao, M., *Journal of Colloid and Interface Science*, **438**, 116-121 (2015).

Chapter 3

One-pot fabrication of palladium nanoparticles captured in mesoporous polymeric monoliths and their catalytic application in C-C coupling reactions

3.1 Introduction

Polymer-based porous hybrid materials (PHMs) are a kind of unique functional materials with metal nanoparticles providing active catalytic site and a porous polymer providing continuous pores for enhanced mass transfer of molecules [1]. PHMs have attracted extensive research interests as heterogeneous catalyst [2-4]. However, the irreversible leaching of metal nanoparticles from porous matrix reduced the reusability and stability of the catalyst, which further limited its practicable applications [5]. Moreover, the preparation of metal nanoparticles and the porous matrix is generally in separated and intricate processes. To overcome these drawbacks, recently some researchers reported the facile preparation of PHMs by the radical-mediated dispersion polymerization or polymerization-induced phase separation method [2,6-7].

Suzuki-Miyaura cross-coupling (SMC) reaction is an important organic synthetic tool for the formation of C-C bond [8]. SMC reaction is usually catalyzed by palladium phosphine, which is toxic and cannot be removed from the reaction media efficiently [9]. In recent years, much effort has been given to heterogeneous catalysts, which could be easily recovered and reused for many cycles. Until now, many heterogeneous catalysts for SMC reaction have been reported by immobilizing Pd in different substrates such as MOF, carbons, clay, montmorillonites, polymers, metal oxides, and mesoporous silica [5,10-16].

In this chapter, a new method for fabricating palladium nanoparticles (PdNPs) captured in a mesoporous poly(ethylene-*co*-vinyl alcohol) (EVOH) monolith (PdNPs-EVOH monolith) based on TIPS method was developed. The formation of PdNPs and the monolith was in a simple one-pot process. The monolith exhibited high catalytic performance toward SMC reaction of aryl halide and aryl boronic acid in a water/ethanol mixture. Moreover, the monolith showed high reusability and low PdNPs leaching properties.

3.2 Experimental

Materials

EVOH with ethylene content of 27 mol % was supplied from Sigma. Glutaraldehyde (GA), isopropanol (IPA), acetone, hydrochloric acid, and palladium (II) chloride ($PdCl_2$) were purchased from Wako Co. All reagents were used as received without further purification.

Instrumentations

Scanning electron microscope (Hitachi Co., SU3500) was used to observe the monolith at an accelerating voltage of 15 kV. Before measurements, the monolith was sputtered with pure gold in vacuo. A NOVA-4200e surface area & pore size analyzer (Quantachrome Instruments) was applied to measure the nitrogen adsorption/desorption isotherms of the monolith at 77 K. The Brunauer Emmett Teller (BET) method and non-local density functional theory (NLDFT) method were applied to establish the specific surface area and the pore size distribution plot, respectively. Induced coupled plasma-atom emission spectrometry (ICP-AES, an ICP-7510 Shimadzu sequential plasma spectrometer) was used to measure the palladium concentration. Energy dispersive X-ray spectrometric (EDX) measurement was carried out by using an energy dispersive X-ray

spectrometer (Hitachi Miniscope TM3000). Gas chromatograph (Shimadzu GC-2014) was applied for the gas chromatographic (GC) studies. Transmission electron microcopy (TEM) image of the monolith was recorded in a transmission electron microscope (Hitachi H-7650). ^{1}H nuclear magnetic resonance (NMR) spectra were recorded with an NMR spectrometer (Bruker BioSpin, Bruker DPX-400) using tetramethylsilane as the internal standard. Wide-angle X-ray diffraction (XRD) was measured on an X-ray diffractometer (Shimadzu XRD-6100) over the 2θ range from 10° to 80°.

Fabrication of PdNPs-EVOH monolith

A general procedure for the fabrication of a mesoporous PdNPs-EVOH monolith is illustrated in Fig. 3-1. The EVOH solution was prepared by dissolving EVOH (300 mg) in a mixed solvent of IPA (1.3 mL) and water (0.7 mL) at 75 ^{o}C. Ten mg of $PdCl_2$ was added to the solution and solution was stirred for 6 h to ensure the complete transition of Pd^{2+} to Pd. Then, the solution was cooled at 4 ^{o}C under air to form the monolith. The obtained monolith was immersed into a large amount of acetone to remove the embedded solvent molecules and subsequently dried under vacuum.

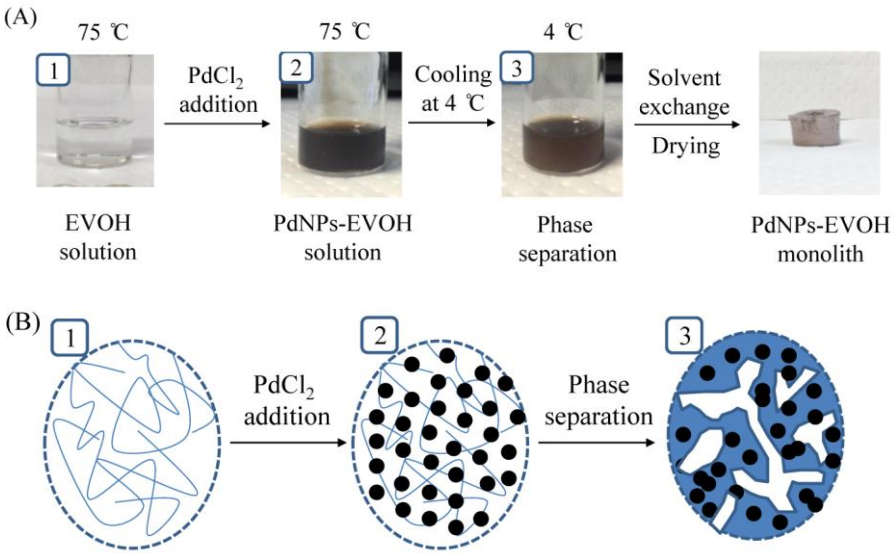

Fig. 3-1 Fabrication procedure of PdNPs-EVOH monolith (A) and schematic of the formation of PdNPs (B).

To prepare the monolith insoluble in common organic solvents, the PdNPs-EVOH monolith was cross-linked by using GA. The cross-linking procedure is as follows. The monolith (200 mg) was immersed to 15 mL of GA aqueous solution (25 % (v/v %)), and 0.1 mL of hydrochloric acid (6.0 M) was added as catalyst. The reaction was carried out at 25 ^{o}C. After 12 h, the monolith was washed by acetone and subsequently dried under vacuum for further applications.

C-C cross coupling reaction with PdNPs-EVOH monolith

A mixture of aryl halide (1.0 mmol), aryl boronic acid (1.5 mmol), potassium carbonate (2.0 mmol), and PdNPs-EVOH monolith (40 mg) in a water/ethanol mixed solvent (3.0 mL, 1:1 (v/v)) was heated at 55 ^{o}C for 6 h. Progress of the reaction was monitored by GC at regular intervals. At the end of the reaction, the catalyst was first separated out by filtration and washed with ethyl acetate four times (5.0 mL x 4). The filtrate was collected and washed with water to remove the excess K_2CO_3. Afterwards, it was washed with brine and dried over $MgSO_4$. The solvent was then evaporated under reduced pressure. The residue was purified by recrystallization using n-hexane/ethyl acetate mixture to give the desired product, which was analyzed by GC and/or ^{1}H NMR. All of the products were known and reported in the literatures. The spectroscopic data (^{1}H NMR) of these products are consistent with those reported values.

Reusability

Iodobenzene and phenylboronic acid were used for evaluation of the reusability for the present monolith catalyst. The reaction condition was the same as that mentioned above. After the first cycle of the SMC reaction, the PdNPs-EVOH monolith was recovered by simple filtration, washed repeatedly with ethyl acetate (5.0 mL x 4) and water (5.0 mL x 5). It was subsequently dried under vacuum at room temperature. The recovered PdNPs-EVOH monolith was transferred into the new substrate solution, which

was heated at 55 ^{o}C. The product was isolated according to the above-mentioned procedures. The catalyst was collected and reused for the next run.

3.3 Results and discussion

Fabrication and characterizations of PdNPs-EVOH monolith

Fig. 3-1 shows a schematic of the proposed method to fabricate PdNPs-EVOH monolith. $PdCl_2$ was added into the EVOH solution in a mixed solvent of IPA and water at 75 ^{o}C. This temperature was chosen because it is the lowest temperature at which EVOH is soluble in the solvent. Due to the reduction of Pd^{2+} to Pd by IPA, the solution transferred from transparence to black color immediately (less than 1 min). The formed Pd nanoparticles were considered to be stabilized by EVOH. We confirmed that aggregated large particles were formed in the solution without EVOH. The reduction reaction was performed for 12 h. Afterwards, the solution was kept at 4 ^{o}C for the phase separation. In this process, the porous monolith was formed and Pd nanoparticles were captured inside the monolith at the same time. After drying, the monolith transferred from black color to gray color. The monoliths again returned to black color by the immersion in a solvent. The color of the monoliths was considered to be strongly related to the electronic state of the Pd atoms [6]; the gray color suggests the existence of Pd in the monolith.

In order to improve solvent tolerance of the monolith toward common organic solvents, the PdNPs-EVOH monolith was cross-linked by GA. FT-IR analysis of the product shows the existence of the unreacted aldehyde group (1720 cm^{-1}), strongly suggesting the successful cross-linking of PdNPs-EVOH monolith (data not shown). In this new method, the formation of PdNPs and the monolith was in a simple one-pot process. Moreover, the present method could be easily applied for the large-scale production of the catalyst, which is highly significant for industrial applications of SMC

Fig. 3-2 shows the SEM image of the PdNPs-EVOH monolith. The SEM image clearly indicates the three-dimensional open macropore structure of the monolith, although the nanoparticles cannot be found in the SEM level. Interestingly, the morphology of the monolith hardly affected the hybrid formation of the nanoparticles and EVOH; the morphology of the present monolith was very similar to that of the EVOH monolith (data not shown).

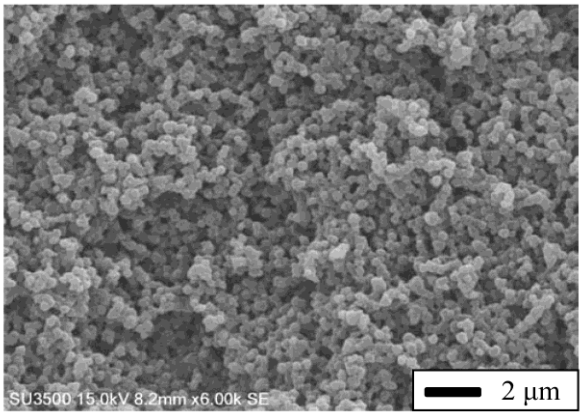

Fig. 3-2 SEM image of the PdNPs-EVOH monolith.

The nitrogen adsorption/desorption isotherms for the monolith exhibited a typical V isotherm with a relatively wide type H1 hysteresis loop, which is the characteristic of the mesoporous structure (Fig. 3-3). The formation of mesopores in the monolith was also

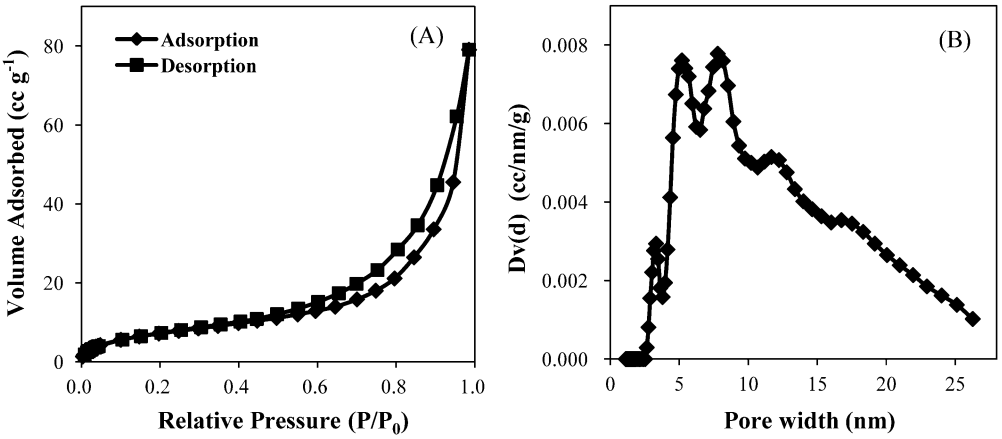

Fig. 3-3 Nitrogen adsorption-desorption isotherm of the PdNPs-EVOH monolith (A) and pore size distribution of the monolith by NLDFT method (B).

proved by the pore size distribution (PSD) plot, which was obtained by using the non-local density functional theory (NLDFT) method. The specific surface area was determined as 57 m^2 g^{-1} by multi-point BET method. These data indicate the PdNPs-EVOH monolith had

relatively uniform mesopores and macropores. The existence of mesopores and macropores enables the capture of Pd nanoparticles and the fast flow through of reaction solution, respectively.

The diameters of PdNPs were mostly located in the range of 5-10 nm, although the particle size distribution is relatively broad (Fig. 3-4). The homogeneous distribution of PdNPs inside the monolith was confirmed by EDX analysis (Fig. 3-5). The existence of PdNPs was further confirmed by wide angle XRD measurement. EVOH monolith and PdNPs-EVOH monolith shared the same peak at 19.8° (Fig. 3-6). Apart from this peak, three diffraction peaks appeared at 2θ=40.0°, 46.5°, and 67.8°, which could be assigned to the (111), (200), and (220) facet diffractions of face-centered cubic Pd, respectively [17].The (111) facet of Pd is considered as the best surface for catalytic application [6].

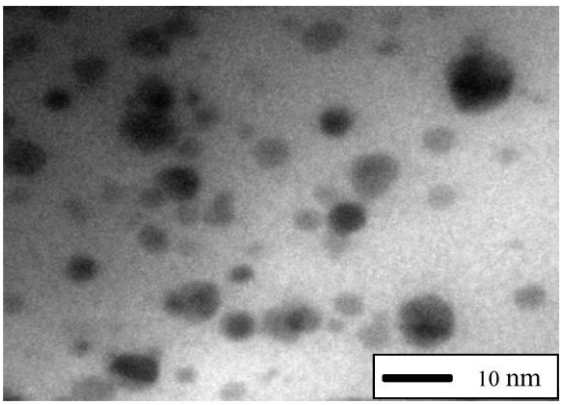

Fig. 3-4 TEM image of the created PdNPs in the PdNPs-EVOH monolith.

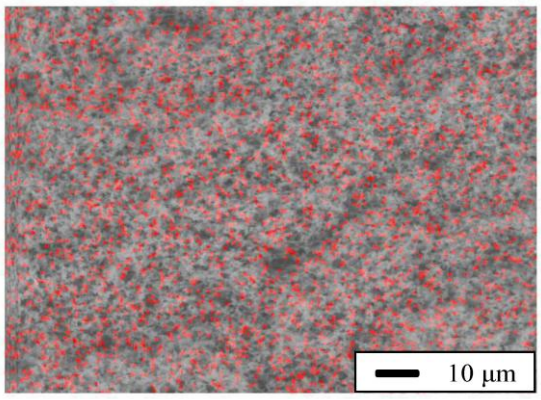

Fig. 3-5 EDX elemental map of Pd in the PdNPs-EVOH monolith.

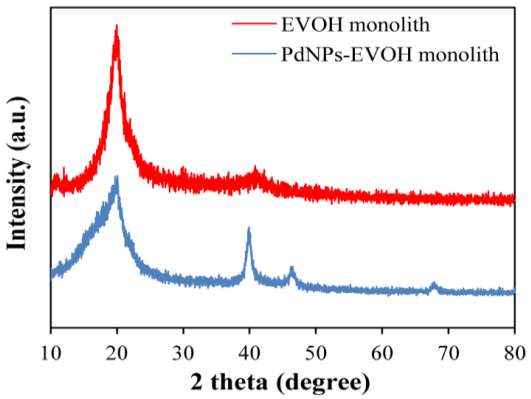

Fig. 3-6 XRD patterns of EVOH monolith (▬) and PdNPs-EVOH monolith (▬).

Catalysis of PdNPs-EVOH monolith

Catalytic performance of the PdNPs-EVOH monolith was studied in a C-C bond forming reaction. Phenylboronic acid and iodobenzene were selected as model substrates and potassium carbonate as base for SMC reaction. At first we measured the yield of SMC reaction in a water/ethanol mixed solvent (3.0 mL, 1:1 (v/v)) with various reaction times (Fig. 3-7). The maximum yield was found after 6 h, which suggests the high efficiency of the present monolith.

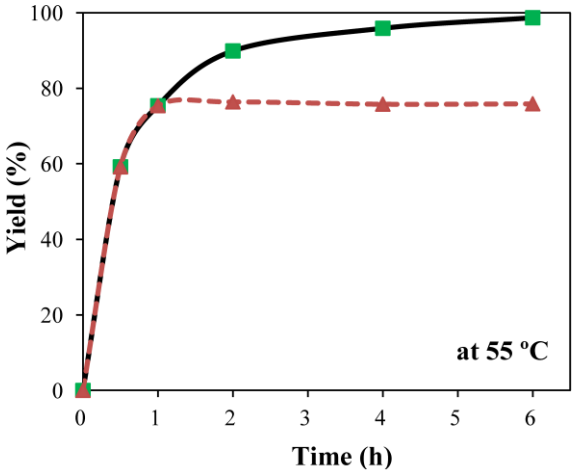

Fig. 3-7 Time-course profile (▬) and hot-filtration study (▬) of SMC reaction over the PdNPs-EVOH monolith.

To investigate the generality of this protocol, various aryl halides and aryl boronic acids were tested under the optimized reaction conditions. The results are summarized in Table 3-1. A variety of aryl halides and aryl boronic acids were successfully coupled to afford the desired products. Aryl halides having bromo and iodo were equally effective in this reaction condition. Aryl halides having electron donating or withdrawing substituent gave the products in excellent yields (90-99 %) with high turn over number (TON) values.

One of the most important concerns about heterogeneous catalysts employed in liquid phase reactions is the catalyst stability. Therefore, we addressed the issue of reusability of the PdNPs-EVOH monolith. The catalyst could be simply separated from the reaction mixture by filtration and reused in another batch of SMC reaction after drying under vacuum. A plot of yield versus the number of reaction cycle for SMC reaction of iodobenzene and phenylboronic acid in the presence of potassium carbonate at 55 ^{o}C is shown in Fig. 3-8. The same reaction procedure followed five times but negligible

decrease of yield was observed under this reaction condition.

Table. 3-1 C-C cross-coupling reaction between various aryl halides and aryl boronic acids using PdNPs-EVOH monolith as catalyst[a]

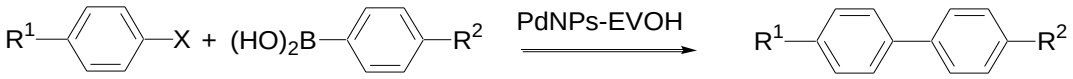

Entry	X	R^1	R^2	Time/h	Yield (%)[b]	TON
1	I	H	H	6	99	122
2	I	OCH_3	H	6	95	117
3	I	$COCH_3$	H	6	99	122
4	I	$COCH_3$	CH_3	6	99	122
5	I	H	CH_3	6	95	117
6	I	CH_3	CH_3	6	97	119
7	Br	NO_2	CH_3	7	90	111
8	Br	NO_2	H	7	99	122
9	Br	$COCH_3$	H	7	99	122
10	Br	$COCH_3$	CH_3	7	98	120

[a]Reaction conditions: aryl halide (1.0 mmol), aryl boronic acid (1.5 mmol), K_2CO_3 (2.0 mmol), PdNPs-EVOH monolith (40 mg), and 3.0 mL of water-ethanol (1:1 (v/v)) at 55 ^oC.
[b]Yield determined by GC.

To verify heterogeneity of the catalyst, i.e. whether the PdNPs-EVOH monolith was truly functioned in a heterogeneous manner, a hot filtration test was performed. The catalyst was separated under the hot condition from the reaction mixture of iodobenzene and phenylboronic acid after 2 h by simple filtration. The filtrate was allowed to be reacted up to the completion of the reaction (6 h). In this case, no change in conversion

was observed (Fig. 3-7), suggesting that the present catalyst is heterogeneous in nature.

The Pd content in the filtrate of the reaction mixture was measured by ICP-AES analysis, which showed that the Pd amount was below the detectable limit. These data strongly suggest that PdNPs hardly leached out from the PdNPs-EVOH monolith during the SMC reaction.

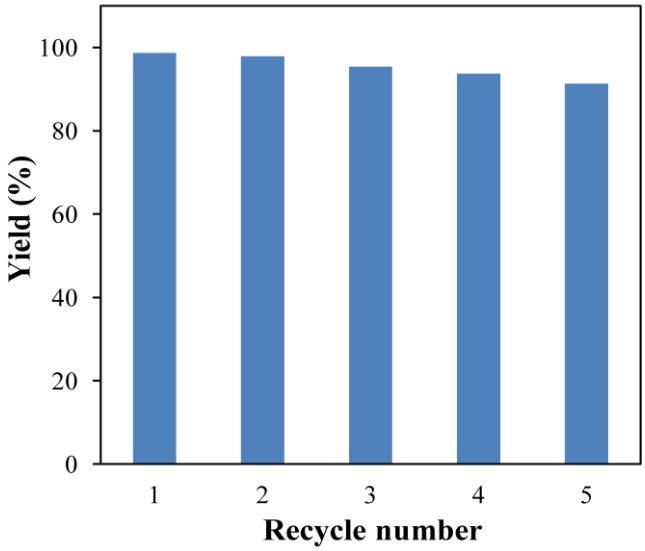

Fig. 3-8 Reusability of the PdNPs-EVOH monolith for C-C coupling reaction of iodobenzene and phenylboronic acid.

3.4 Conclusions

In summary, a one-pot method to fabricate PdNPs captured in a mesoporous monolith has been developed by using TIPS method. The resultant monolith had mesoporosity with high specific surface area. The created PdNPs with diameters of 5 nm-10 nm were dispersed uniformly in the PdNPs-EVOH monolith. The monolith showed outstanding SMC catalytic performance toward various substrates. Moreover, the monolith exhibited very low leaching properties and high reusability. The present 3-D porous catalyst with the superiority of high catalysis activity, excellent stability, large-scale and low-cost production has great potential for practical catalysis applications.

3.5 References

1. Lee, A.; Dubinsky, S.; Tumarkin, E.; Moulin, M.; Beharry, A. A.; Kumacheva, E., *Advanced Functional Materials*, **21**, 1959-1969 (2011).
2. Dubinsky, S.; Petukhova, A.; Gourevich, I.; Kumacheva, E., *Chemical Communications*, **46**, 2578-2580 (2010).
3. Zhu, T.; Row, K. H., *Journal of Separation Science*, **35**, 1294-1302 (2012).
4. Wang, B.; de Godoi, F. C.; Sun, Z.; Zeng, Q.; Zheng, S.; Frost, R. L., *Journal of Colloid and Interface Science*, **438**, 204-211 (2015).
5. Li, Z.; Liu, J.; Huang, Z.; Yang, Y.; Xia, C.; Li, F., *ACS Catalysis*, **3**, 839-845 (2013).
6. Ogasawara, S.; Kato, S., *Journal of the American Chemical Society*, **132**, 4608-4613 (2010).
7. Kong, H.; Jang, J., *Chemical Communications*, 3010-3012 (2006).
8. Nandi, M.; Uyama, H., *RSC Advances*, **4**, 20847-20855 (2014).
9. Sivudu, K. S.; Reddy, N. M.; Prasad, M. N.; Raju, K. M.; Mohan, Y. M.; Yadav, J. S.; Sabitha, G.; Shailaja, D., *Journal of Molecular Catalysis A: Chemical*, **295**, 10-17 (2008).
10. Linares, N.; Serrano, E.; Rico, M.; Mariana Balu, A.; Losada, E.; Luque, R.; García-Martínez, J., *Chemical Communications*, **47**, 9024-9035 (2011).
11. Kundu, D.; Patra, A. K.; Sakamoto, J.; Uyama, H., *Reactive and Functional Polymers*, **79**, 8-13 (2014).
12. Chen, L.; Gao, Z.; Li, Y., *Catalysis Today*(2014).
13. Contin, A.; Biffis, A.; Sterchele, S.; Dörmbach, K.; Schipmann, S.; Pich, A., *Journal of Colloid and Interface Science*, **414**, 41-45 (2014).
14. Jana, S.; Dutta, B.; Bera, R.; Koner, S., *Inorganic Chemistry*, **47**, 5512-5520 (2008).
15. Varadwaj, G. B. B.; Rana, S.; Parida, K., *Journal of Physical Chemistry C*, **118**,

1640-1651 (2014).

16. Gniewek, A.; Ziółkowski, J. J.; Trzeciak, A. M.; Zawadzki, M.; Grabowska, H.; Wrzyszcz, J., *Journal of Catalysis*, **254**, 121-130 (2008).
17. Teranishi, T.; Miyake, M., *Chemistry of Materials*, **10**, 594-600 (1998).

Chapter 4

Immobilization of catalase onto hydrophilic poly(ethylene-*co*-vinyl alcohol) monoliths

4.1 Introduction

In chapter 1, EVOH-based monolith has been fabricated by using TIPS technique for the first time. The EVOH monolith possessing hydrophilic hydroxyl groups has many superior properties over other hydrophobic polymers for enzyme immobilization [1]. Moreover, the hydroxyl groups have been activated by CDI for futher biomolecules immobilization.

Catalase is widely used in industry, including removal of hydrogen peroxide from milk or fabrics [2-3]. It is also employed for the production of gluconic acid when associated with glucose oxidase [4-5]. Moreover, it can be used for hydrogen peroxide biosensor [6] or catalase test. Until now, numerous matrixes have been used for the immobilization of catalase [7-10]. However, the immobilization of catalase onto polymeric monolithic materials has never been reported. The advantage of monolithic materials for enzyme immobilization is that they have a continuous pores structure, allowing flow-through of reaction solution [11]. Moreover, they can be fabricated into different shapes by cutting or cast for designing various kinds of reactors [11].

In this chapter, the immobilization of catalase onto the CDI-EVOH monolith will be reported. The effects of pH and temperature on the activity of free and immobilized catalase were investigated by measuring the efficiency of them for the decomposition of hydrogen peroxide. Furthermore, the thermal stability and reusability of the immobilized catalase were discussed.

4.2 Experimental

Materials

EVOH with ethylene contents of 27 mol%, catalase, and QuantiPro^{TM} BCA Assay Kit were supplied by Sigma Co. Carbonyldiimidazole (CDI), isopropanol (IPA), hydrogen peroxide, acetone, and acetonitrile (ACN) were purchased from Wako Co. All reagents were used as received without further purification.

Instruments

HITACHI S-3500 was used to observe the scanning electron microscope (SEM) images of the monoliths at 15 kV. Before observation, the monoliths were sputtered with pure gold in vacuo. UV was measured by a HITACHI U2810 spectrometer.

Preparation of EVOH monoliths

EVOH monoliths were prepared according to our reported method [13]. The typical procedure to prepare EVOH monoliths is as follows: A mixed solvent of IPA (0.65 mL) and water (0.35 mL) was used to dissolve 150 mg of EVOH pellet at 75 ºC. Then the solutions were cooled at 20 ºC to induce phase separation. Subsequently, the monoliths were immersed into acetone for solvent replacement and dried under vacuum.

Immobilization of catalase

EVOH monolith (0.10 g) was immersed in ACN solution (5.0 mL) in the presence of CDI (40 mg/mL). After reaction for 4 h at 40 ºC, the monolith was washed with extra amount of acetone and dried under vacuum. The CDI modified EVOH monolith (CDI-EVOH monolith) was stored at 4 ºC for further uses.

Catalase immobilization process is as follows: CDI-EVOH monolith (50 mg) was added to 10 mL of catalase solution (0.50 mg/mL) in a phosphate buffer (0.10 M, pH 6.8). The immobilization experiment was conducted at 4 ºC for 12 h. After immobilization, the catalase immobilized EVOH monolith (catalase-EVOH monolith) was removed from the

reaction solution and washed with phosphate buffer (0.10 M, pH 6.8) for at least 3 times. Concentration of catalase in the mixture was determined by bicinchoninic acid (BCA) method [12] using a calibration curve prepared with catalase solution of known concentrations. Scheme 4-1 shows a schematic representation for the activation of EVOH monolith and the immobilization of catalase.

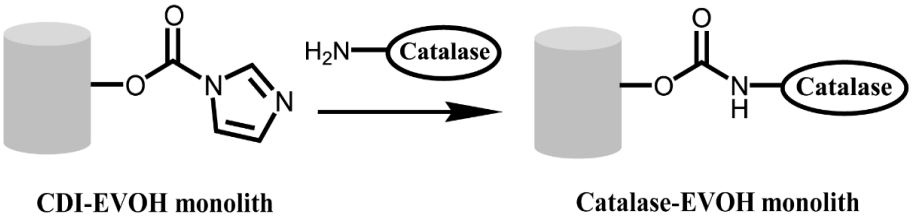

CDI-EVOH monolith **Catalase-EVOH monolith**

Scheme 4-1 Immobilization of catalase onto CDI-EVOH monolith.

Activity assays of free and immobilized catalase

Catalase is efficient in the decomposition of hydrogen peroxide. To determine the activity of free and immobilized catalase, the decrease in the absorbance of hydrogen peroxide at 240 nm was measured. Hydrogen peroxide solutions with the concentration of 2.5-20 mM were used to determine enzyme activity. The activity assays of free and immobilized catalase are as follows: 5.0 mL of hydrogen peroxide solution was equilibrated at 25 ºC for 10 min. Fifty microliter of catalase solution (25 μg/mL) or 20 mg of catalase-EVOH monolith was added to the hydrogen peroxide solution. After 5 min, the reaction was terminated by adding 0.40 mL of HCl solution (1.0 M) or by removal of catalase-EVOH monolith from the reaction solution for free and immobilized enzyme activity assay, respectively. One unit of activity is defined as the decomposition of 1.0 μmol of hydrogen peroxide per minute at 25 ºC and pH 6.8. Relative activity was calculated by comparing the specific activity value with the highest value of each set which was assigned as 100% activity.

To determine the pH and temperature profiles of catalase, the activity assays were

performed over the pH range of 5.0-9.0 and temperature range of 0-65 ºC. The effects of pH on the activity of catalase were determined with 20 mM of hydrogen peroxide solution with different pH at 25 ºC. Temperature profiles of catalase were determined with 20 mM of hydrogen peroxide solution at pH 6.8.

Reusability and thermal stability studies

The reusability and thermal stability of catalase were also determined by the decomposition of hydrogen peroxide. To determine the reusability of immobilized catalase, a piece of catalase-EVOH monolith (20 mg) was added to 5.0 mL of hydrogen peroxide solution (20 mM). After reaction for 5 min, the reaction was terminated by removal of the monolith from the reaction solution. After that, the monolith was washed thoroughly with phosphate buffer (0.10 M, pH 6.8). Activity test and washing cycle was repeated for eleven times. The decrease in the absorbance of hydrogen peroxide at 240 nm due to its decomposition by immobilized catalase was determined spectrophotometrically. Residual activity at each reuse circle was calculated by comparing the activity at each reuse circle with the activity at the 1^{st} circle which was assigned as 100% activity.

Thermal stability of free and immobilized catalase was tested by measuring the residual enzymatic activity at 50 ºC in a phosphate buffer (0.10 M, pH 6.8) for 150 min. Every 30-min time interval, a sample was assayed for its enzymatic activity.

4.3 Results and discussion

Characterizations of EVOH monolith and immobilization of catalase

Interconnected network of macropores with diameter of micron scale were clearly observed from the SEM images. This kind of structure allows reaction solution to flow through the monolith easily. Our previous study illustrated that the monolith also had uniform mesopores, which was large enough for enzyme immobilization [13]. The

combination of macropores and mesopores afforded the EVOH monolith an ideal matrix for enzyme immobilization. Before enzyme immobilization, the hydroxyl groups of the EVOH monolith were activated with CDI in anhydrous ACN solution. The activated EVOH monolith contained imidazolyl carbamate groups which could react with free amino groups in the enzyme. Catalase was immobilized on the activated hydrophilic EVOH monolith. The amount of catalase immobilized onto the EVOH monolith was determined as 6.0 mg catalase/g monolith.

Effects of pH and temperature on activity

The effects of pH on the activity of free and immobilized catalase were performed in a phosphate buffer (0.10 M, pH 6.8) in the pH range of 5.0–9.0 and the results were shown in Fig. 4-1. It could be observed that the pH profile of the immobilized catalase was similar to the free enzyme when pH is higher than 6.8, but much broader when pH is lower than 6.8, probably due to the secondary interaction between the enzyme and the monolith when pH is lower than 6.8 [13-14]. The maximum activity was observed at pH 6.8 for both free and immobilized catalase. The optimum pH value of immobilized enzyme

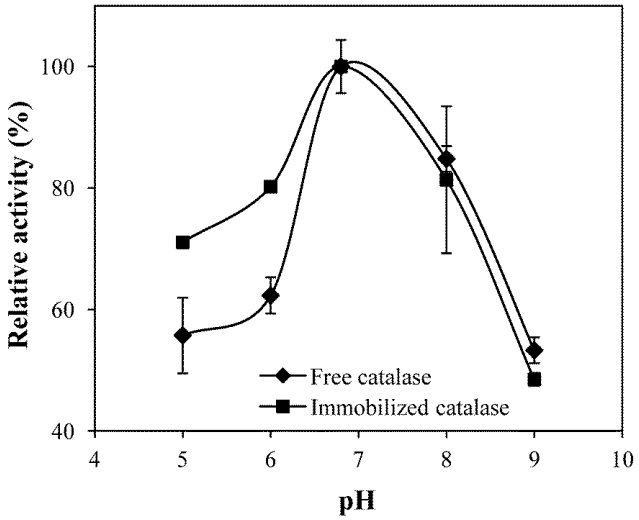

Fig. 4-1 Relative enzyme activity as a function of pH for free (◆) and immobilized (■) catalase.

compared with that of free enzyme is determined by the surface and residual charges on the immobilization matrix [15].

To determine the temperature profile, the activity of free and immobilized catalase was investigated in a phosphate buffer (0.10 M, pH 6.8) at various temperatures (0–65 ºC). As it can be seen in Fig. 4-2, the free and immobilized catalase exhibited similar temperature profile. The optimum temperature values for the free and immobilized catalase were found as 30 ºC. The activity of both the free and immobilized catalase decreased rapidly at temperature higher or lower than 30 ºC. Generally, effects of temperature on the rates of enzyme-catalyzed reactions do not give much information on the mechanism of enzyme catalysis. But, these effects could indicate the structural changes in enzyme. The similar temperature profile of the free and immobilized catalase indicated that the catalase could retain its structure after immobilization.

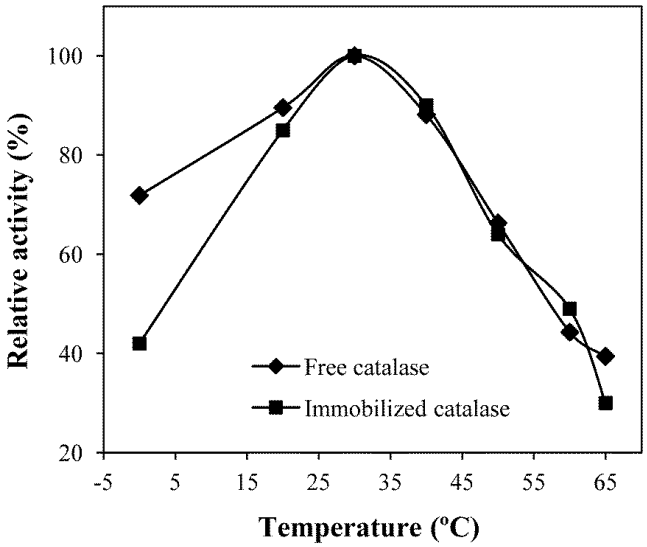

Fig. 4-2 Relative enzyme activity as a function of temperature for free (◆) and immobilized (■) catalase.

Thermal stability measurements for free and immobilized catalase

Thermal stability of free and immobilized catalase was determined by measuring the residual enzymatic activity at 50 ºC in a phosphate buffer (0.10 M, pH 6.8) for 150 min. Both the residual enzymatic activity of free and immobilized catalase decreased with increasing of incubation time. This may be because that high temperature induced conformational changes of the catalase, and subsequently, inactivation of it. After incubation for 150 min at 50 ºC, residual enzymatic activities for the free catalase and immobilized catalase were found as 32% and 57% of their original activity, respectively (Fig. 4-3). These results indicated that the thermal stability of immobilized catalase was higher than that of free catalase. It is probably because that EVOH monolith as a matrix preserved tertiary structure of the catalase and this protected the catalase from conformational changes caused from microenvironment changes.

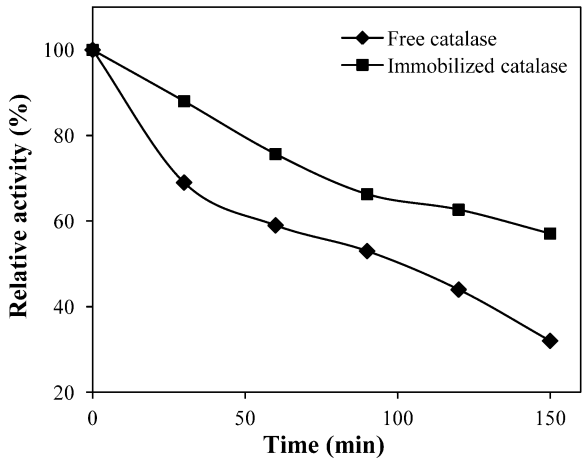

Fig. 4-3 Thermal stability of free (◆) and immobilized (■) catalase at 50 ºC.

Reusability of immobilized catalase

One of the important advantages of immobilized enzyme is that it could be reused for many times. The reusability of immobilized catalase is showed in Fig. 4-4. The immobilized catalase retained 75% of its initial activity after being used for eleven times.

The stable covalent bonds between catalase and EVOH monolith, was probably the reason for this high recycling stability. The high reusability of immobilized catalase is vital in consideration of their potential industrial applications.

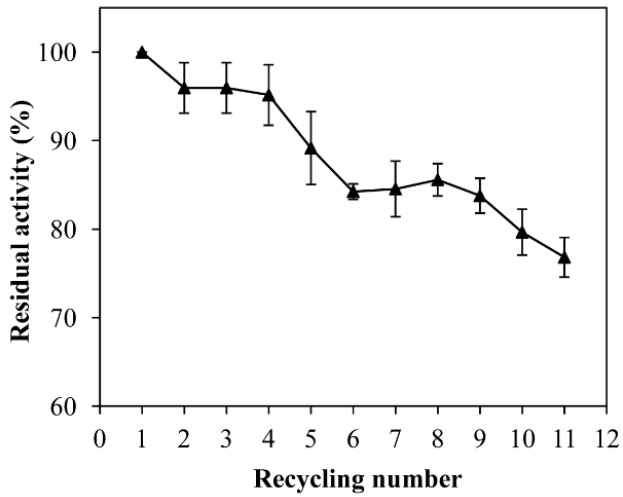

Fig. 4-4 Reusability of immobilized catalase.

4.4 Conclusions

In conclusion, hydrophilic EVOH monoliths have been prepared by a TIPS method. The monoliths were activated by CDI for catalase immobilization. Optimum pH value was found as 6.8 and optimum temperature value was determined as 30 ºC for both free catalase and immobilized catalase. The immobilized catalase retained 75% of its initial activity after eleven successive cycles of decomposition of hydrogen peroxide. The hydrophilic catalase-EVOH monolith with a three dimensional continuous porous structure will find valuable applications in biotechnology.

4.5 References

1. Kumar, G. S. V.; Kumar, K. S., *Journal of Applied Polymer Science*, **97**, 8-19 (2005).
2. Alston, M.; Willetts, A.; Wells, A., *Organic Process Research and Development*, **6**, 505-508 (2002).
3. Ikemura, M.; Nishikawa, M.; Hyoudou, K.; Kobayashi, Y.; Yamashita, F.; Hashida, M., *Molecular Pharmaceutics*, **7**, 2069-2076 (2010).
4. Nakao, K.; Harada, T.; Furumoto, K.; Kiefner, A.; Popovic, M., *Canadian Journal of Chemical Engineering*, **77**, 816-825 (1999).
5. Godjevargova, T.; Dayal, R.; Turmanova, S., *Macromolecular Bioscience*, **4**, 950-956 (2004).
6. Yut, A.; Caruso, F., *Analytical Chemistry*, **75**, 3031-3037 (2003).
7. Zhang, J.; Zhou, X.; Wang, D.; Wang, Y.; Wang, H.; Li, Q.; Tan, S., *Journal of Molecular Catalysis B: Enzymatic*, **97**, 80-86 (2013).
8. Alptekin, O.; Tükel, S. S.; Yildirim, D.; Alagöz, D., *Journal of Molecular Catalysis B: Enzymatic*, **64**, 177-183 (2010).
9. Alptekin, Ö.; Seyhan Tükel, S.; Yildirim, D.; Alagöz, D., *Enzyme and Microbial Technology*, **49**, 547-554 (2011).
10. Netto, C. G. C. M.; Toma, H. E.; Andrade, L. H., *Journal of Molecular Catalysis B: Enzymatic*, **85-86**, 71-92 (2013).
11. Nandi, M.; Okada, K.; Uyama, H., *Functional Materials Letters*, **4**, 407-410 (2011).
12. Smith, P. K.; Krohn, R. I.; Hermanson, G. T.; Mallia, A. K.; Gartner, F. H.; Provenzano, M. D.; Fujimoto, E. K.; Goeke, N. M.; Olson, B. J.; Klenk, D. C., *Analytical Biochemistry*, **150**, 76-85 (1985).
13. Le-Tien, C.; Millette, M.; Lacroix, M.; Mateescu, M. A., *Biotechnology and Applied Biochemistry*, **39**, 189-198 (2004).

14. Emregul, E.; Sungur, S.; Akbulut, U., *Food Chemistry*, **97**, 591-597 (2006).

15. Akgo, S.; Oztiirk, N.; Denizli, A., *Journal of Applied Polymer Science*, **114**, 962-970 (2009).

Chapter 5

Facile fabrication of mesoporous poly(ethylene-*co*-vinyl alcohol)/chitosan blend monoliths

5.1 Introduction

Chitosan is a linear polysaccharide commercially produced by the deacetylation of chitin. It has great advantages in the removal of heavy metal ions which tend to accumulate in livings organisms and are highly toxic to environment [1-2]. At the same time, chitosan is especially suitable for bio-related applications such as enzyme immobilization, drug delivery, and protein separation for its beneficial properties including biodegradation, hydrophilicity, biocompatibility, and ease of chemical modification [3-6]. Mesopores with pore diameters in the range of 2 to 50 nm show high efficiency for the adsorption of both small and large molecules [7-9]. Therefore, chitosan-based monoliths with mesoporous structure are highly demanded for the above applications.

Generally, chitosan-based materials with macroporous structure in the type of bead [10-11], gel [12-13], foam [14], and membrane [15] were prepared by using the methods such as freeze-drying, phase-inversion, or porogen-leaching. In contrast, little research was done on the fabrication of chitosan-based monolithic materials [16]. Most importantly, a mesoporous structure has never been achieved in those materials. A potential route to the fabrication of chitosan monoliths with mesoporous structure is through TIPS technique using chitosan itself as a precursor [17]. In this technique, a relatively high polymer concentration is necessary to ensure sufficient polymer molecules in a space. However, chitosan solution has an extremely high viscosity at high concentration, making it difficult to form a chitosan monolith. Moreover, it is not easy to control the formation of a

mesoporous structure in a monolith. Our hypothesis was that blend with other polymers may be an effective way to fabricate a mesoporous monolith containing chitosan. Successful preparation of the mesoporous chitosan would not only be scientific interesting, but also expand the applications of chitosan to a much broader area.

This chapter will describe the exploration of the hypothesis. We selected EVOH as the main compound of the monolith. Because this polymer was proved to be able to form a mesoporous structure easily in the TIPS process and the hydroxyl groups could form tough hydrogen bonding with chitosan. Moreover, it has many advantages for bio-related applications including biocompatibility, hydrophilicity, thermal stability, and chemical resistance. We anticipated that phase separation of a solution containing both EVOH and chitosan could induce the formation of a monolith with mesoporous structure and interesting morphology. We describe as part of this research the application of the mesoporous monolith for the adsorption and desorption of heavy metal ions to verify the efficiency of chitosan.

5.2 Experimental

Materials

EVOH with ethylene contents of 27 mol% was supplied from Sigma Co. Acetate buffer solution (0.10 M, pH 5.0) was purchased from Nacalai Tesque. Copper chloride, nickel chloride, cobalt chloride, isopropanol (IPA), acetone, epichlorohydrin, and chitosan were purchased from Wako Co. Degree of deacetylation for the chitosan was calculated as 75% by the elemental analysis results using the formula described in the literature (Kasaai, Arul & Charlet, 2000). The weight average molecular weight was measured as 1.4×10^4 by size-exclusion chromatographic (SEC) analysis. Viscosity of the chitosan with a concentration of 5.0 g/L at 20 ^{o}C is 0.80-1.5 Pa.s. All reagents were used as received

without further purification.

Fabrication and cross-linking of EVOH/chitosan blend monoliths

The general procedure for the fabrication of the blend monoliths is illustrated in Fig. 5-1. The following experiment process shows the fabrication of a blend monolith with total polymer concentration of 70 mg/mL and EVOH weight ratio of 70 wt%. Firstly, 42 mg of chitosan was dissolved in 1.1 mL of water containing 2.0% (v/v) of acetic acid under air. Ninety eight milligram of EVOH and 0.90 mL of IPA were added to the solution. The solution was heated at 75 ^{o}C to dissolve EVOH. Afterwards, the solution was cooled at 20 ^{o}C to form the blend monolith, which was immersed into a large amount of acetone to remove the embedded solvents and subsequently dried under vacuum.

To measure the metal ions desorption ability in acid solution, a blend monolith was cross-linked by epichlorohydrin using the following procedure [18]. The blend monolith (0.30 g) was added to 40 mL of epichlorohydrin aqueous solution (10^{-2} M; pH 10). After heating at 50 ^{o}C for 2 h, the product was washed by acetone and dried under vacuum. By measuring the weights of a cross-linked blend monolith in its dry state and wet (swollen) state, the weight swelling ratio was calculated as 450% [19]. Moreover, the total porosity was calculated as 83% by gravimetry using the equation described in the literature [20].

Instruments

Morphologies of the monoliths were observed by scanning electron microscope (SEM, Hitachi Co., SU3500) at 15 kV. For SEM examination, the monoliths were cut into small pieces, and sputtered with gold under vacuo. The nitrogen adsorption/desorption isotherms for the monoliths were measured by a NOVA-4200e Surface Area & Pore Size Analyzer (Quantachrome Instruments) at 77 K. The specific surface area and the pore size distribution (PSD) plots were determined by the Brunauer Emmett Teller (BET) method and non-local density functional theory (NLDFT) method, respectively. The composition

of the monolith was determined by elemental analysis (Yanaco New Science Inc. CHN corder MT-5). Metal ion concentrations were measured by induced coupled plasma-atom emission spectrometry (ICP-AES, an ICP-7510 Shimadzu sequential plasma spectrometer). FT-IR measurement was performed by Thermo Scientific (Yokohama, Japan) Nicolet iS5 with the attenuated total reflectance method. Size-exclusion chromatographic (SEC) analysis was carried out at 40 °C using an apparatus (Tosoh GPC-8020) equipped with refractive-index (RI) and TSKgel α-M column. Acetate buffer solution (0.10 M, pH 5.0) was used as eluent at a flow rate of 1.0 mL/min. The calibration curves were obtained using poly(ethylene oxide) standards.

Bath adsorption experiments

Stock solutions of Cu^{2+}, Ni^{2+}, and Co^{2+} were prepared by using copper chloride, nickel chloride, and cobalt chloride, respectively. The stock solutions were then diluted to give standard solutions of appropriate concentrations. Fifty milligram of the blend monolith (total polymer concentration: 70 mg/mL; EVOH weight ratio: 70 wt%) was added to 5.0 mL of metal ion solution (0.50 g/L). After adsorption, the concentrations of residual metal ion solutions were measured by ICP.

To test the desorption of Cu^{2+}, the cross-linked blend monolith (0.15 g) was added to Cu^{2+} solution (3.0 g/L) and kept for 24 h under gentle shaking. The monolith was then immersed into HCl solution (0.10 M) for the desorption of Cu^{2+}.

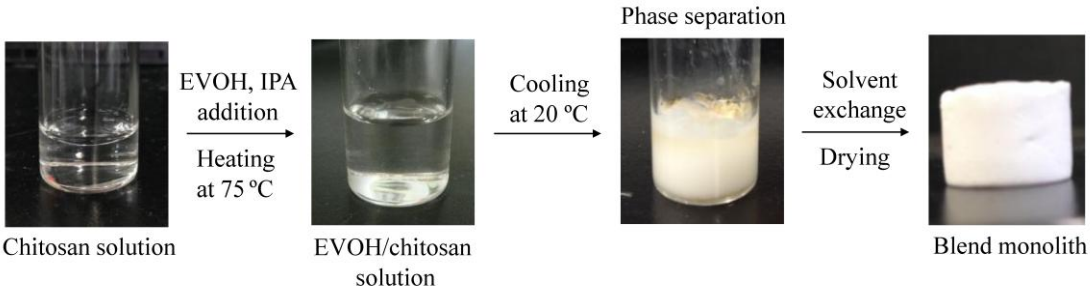

Fig. 5-1 Fabrication procedure of the blend monolith

5.3 Results and discussion

Preparation and characterization of blend monoliths

Even though chitosan is insoluble in a water/IPA mixture, a transparent chitosan/EVOH solution could be obtained by dissolving chitosan in a 2.0% (v/v) acetic acid solution and subsequent addition of EVOH and IPA to the chitosan solution. Our previous results revealed that EVOH monolith could be fabricated from a water/IPA mixture with the water content of 30-55% (v/v) (data not shown). In case of the blend monolith, the water/IPA mixture with the water content of 55% would be the most suitable solvent for the fabrication, since this mixed ratio could blend the highest amount of chitosan.

Besides the water/IPA ratio, the polymer concentrations also affect the formation and morphology of the monolith. The monolith with bicontinuous structure was formed when the ranges of the total polymer concentration and the mixing ratio of EVOH were 70-160 mg/mL and 70-90% (v/v), respectively. These results reveal that chitosan could be incorporated into polymeric monoliths by blending with EVOH.

At low polymer concentration, the monolith was not obtained probably due to the small numbers of the polymer molecules to form the skeleton of monolith in a space. When the total polymer concentration or the ratio of chitosan was higher, the formation of the monolith was not found, which may be because the solution viscosity was very high for the phase separation [21].

Fig. 5-2 shows the adsorption/desorption isotherms of the EVOH/chitosan blend monolith which was prepared under the following conditions: the total polymer concentration was 70 mg/mL and EVOH ratio was 80 wt%. A typical V isotherm with type H1 hysteresis loop in the P/P_0 range from 0.45 to 1.0 was observed from Fig. 5-2 (A), strongly suggesting the formation of a mesopore structure in the monolith. Fig. 5-2 (B)

reveals the PSD result of the blend monolith by applying the NLDFT method, which shows the pores in the range of mesopores (2 ~ 50 nm) with the peak-top pore diameter of ca. 5.0 nm. The specific surface area obtained by BET method was 61 m^2g^{-1}, which indicates the large specific surface area of the present monolith. These data clearly show that the blend monolith had mesopore structure with large specific surface area.

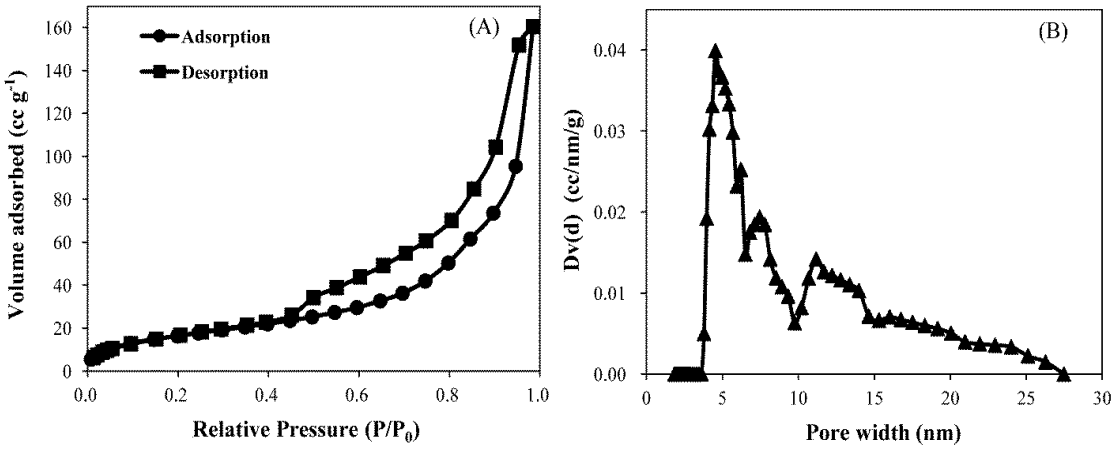

Fig. 5-2 Nitrogen adsorption-desorption isotherms of the blend monolith (A) and pore size distribution of the blend monolith by NLDFT method (B).

Fig. 5-3 shows the SEM images of the blend monolith (without cross-linking). The blend monolith had continues interconnected network structure. It could be found that the inner surface of the blend monolith was rough and a polymer layer was attached on the inner surface. After immersing the blend monolith in an acetate buffer solution of pH 5.0 for several times, the inner surface of the blend monolith became smooth and the attached polymer layer disappeared. These results indicate that the polymer layer was chitosan, because EVOH is water insoluble but chitosan is water soluble at pH<6.0. This phenomenon may be due to the slower phase separation of chitosan than EVOH.

For the purpose of surface modification and/or efficient chitosan utilization, coating of chitosan onto various materials has been extensively studied [22-24]. In this study, chitosan was easily coated on the inner surface of the monolith during the phase

separation process, leading to the efficient usage of reactive primary amine groups in further applications.

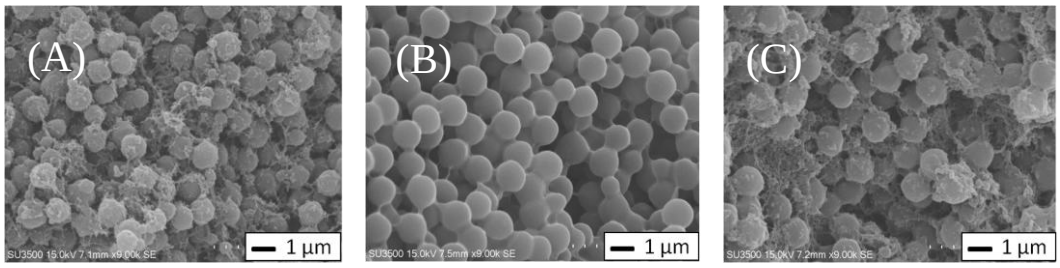

Fig. 5-3 SEM images of blend monolith (A), blend monolith after washing with a buffer of pH 5 (B), and cross-linked blend monolith after washing with a buffer of pH 5 (C).

Fig. 5-4 presents the FT-IR spectra of EVOH, chitosan, and blend monolith. The distinguished adsorption bands of EVOH are the antisymmetric and symmetric C–H stretching vibration of the methanediyl groups at 2917 cm^{-1} and 2849 cm^{-1}, respectively. Meanwhile, the distinguished adsorption band of chitosan due to the amide group is found at 1650 cm^{-1}. In the EVOH/chitosan blend monolith, both distinguished adsorption bands of EVOH and chitosan clearly appear, strongly suggesting that the obtained monolith contained both polymers.

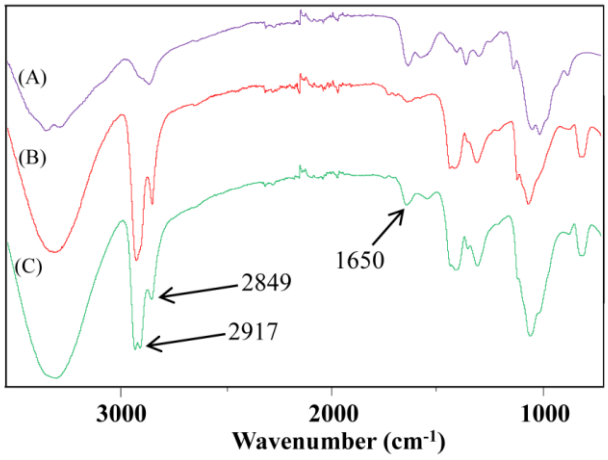

Fig. 5-4 FT-IR spectra of EVOH (A), chitosan (B), and blend monolith (C).

Results of elemental analysis are summarized in Table 5-1. With increasing of the chitosan ratio, the nitrogen contents of the blend monolith increased linearly to the

chitosan ratio. This data indicates that chitosan was quantitatively introduced into the monolith, which may due to the formation of strong hydrogen bonding between EVOH and chitosan.

Table 5-1. Elemental analysis results.

EVOH/chitosan (wt/wt %)	Elemental compositions (wt %)		
	H	C	N
90/10	9.53	57.1	0.70
80/20	8.92	55.4	1.44
70/30	8.90	53.9	2.21
0/100	6.78	39.8	7.15

Adsorption and desorption of heavy metal ions

The heavy metal ions adsorption ability of the blend monolith (without cross-linking) was studied. Fig. 5-5 shows the adsorption ability of the blend monolith toward heavy metal ions. The adsorption ability toward Cu^{2+} was the highest. Comparing to other chitosan composites previously reported, our monolith showed the similar behaviors [25]. On the other hand, the EVOH monolith had no chelation ability toward Cu^{2+} (data not shown), supporting the formation of the blend monolith of EVOH and chitosan.

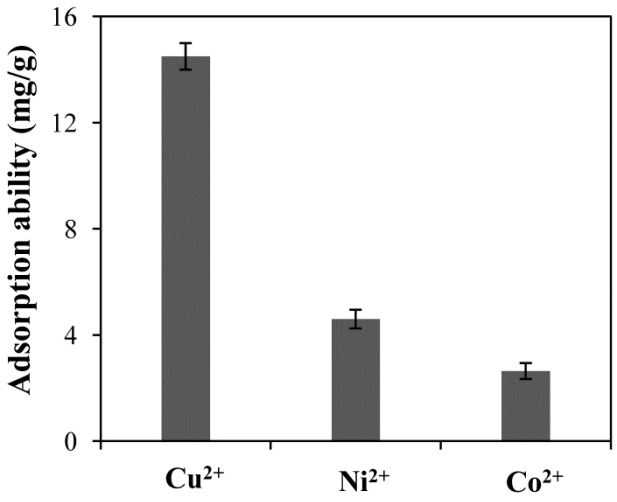

Fig. 5-5 Adsorption of heavy metal ions by the blend monolith.

The desorption of Cu^{2+} from the blend monolith is vital in considering practical chelation applications of the blend monolith [16]. Fig. 5-6 shows photographs of the monolith in the adsorption and desorption process of Cu^{2+}. The white blend monolith became homogenous (both inside and outside) blue after the monolith was kept in Cu^{2+} solution for 24 h. The surface of the obtained monolith turned to light blue after immersing it in HCl solution (0.10 M) even for 10 sec. After 30 min, the inside and outside of the monolith returned to its original white color. This result strongly suggests the desorption of most of the Cu^{2+} from the blend monolith. Additionally, the monolith shape did not change in the processes of adsorption and desorption of heavy metal ions, which is important for applications of the present blend monolith as chelating materials for water purification.

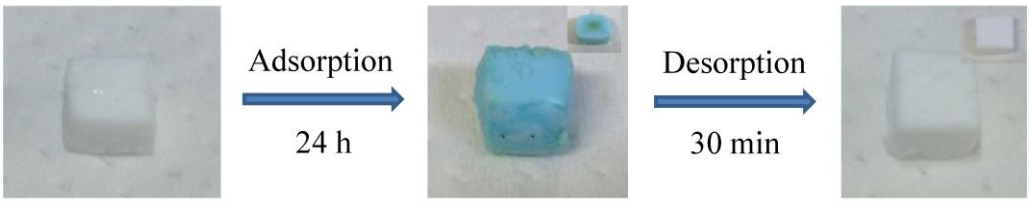

Fig. 5-6 Photographs of the blend monoliths in the processes of adsorption and desorption of Cu^{2+} (inner pictures: inside blend monolith).

5.4 Conclusions

A monolithic material based on biocompatible EVOH and chitosan was fabricated by TIPS for the first time. FT-IR and elemental anyalysis suggest the successful blend of the two polymers. BET results indicate the monolih had relativly high specific area and unifrom mesopore structure. The chitosan layer was interestingly located on the inner surface of the monolith. Additionally, the blend monolith showed good adsorption ability toward heavy metal ions. A combination of unique structural features of monoliths

and primary amine groups of chitosan on the monolith surface will provide various applications such as water treatment, metal recycle, and biomolecules purification.

5.5 References

1. Babel, S.; Kurniawan, T. A., *Journal of Hazardous Materials*, **97**, 219-243 (2003).
2. Crini, G., *Progress in Polymer Science (Oxford)*, **30**, 38-70 (2005).
3. Davydova, V. N.; Volod'Ko, A. V.; Sokolova, E. V.; Chusovitin, E. A.; Balagan, S. A.; Gorbach, V. I.; Galkin, N. G.; Yermak, I. M.; Solov'Eva, T. F., *Carbohydrate Polymers*, **123**, 115-121 (2015).
4. Correia, C. O.; Leite, Á. J.; Mano, J. F., *Carbohydrate Polymers*, **123**, 39-45 (2015).
5. Jiang, L.; Lu, Y.; Liu, X.; Tu, H.; Zhang, J.; Shi, X.; Deng, H.; Du, Y., *Carbohydrate Polymers*, **121**, 428-435 (2015).
6. Zhang, X.; Duan, Y.; Wang, D.; Bian, F., *Carbohydrate Polymers*, **122**, 53-59 (2015).
7. Kawashima, D.; Aihara, T.; Kobayashi, Y.; Kyotani, T.; Tomita, A., *Chemistry of Materials*, **12**, 3397-3401 (2000).
8. Hu, Z.; Srinivasan, M. P.; Ni, Y., *Advanced Materials*, **12**, 62-65 (2000).
9. Ryoo, R.; Joo, S. H.; Kruk, M.; Jaroniec, M., *Advanced Materials*, **13**, 677-681 (2001).
10. Fu, G.; Li, H.; Yu, H.; Liu, L.; Yuan, Z.; He, B., *Reactive and Functional Polymers*, **66**, 239-246 (2006).
11. Mi, F. L.; Shyu, S. S.; Chen, C. T.; Lai, J. Y., *Polymer*, **43**, 757-765 (2001).
12. Kathuria, N.; Tripathi, A.; Kar, K. K.; Kumar, A., *Acta Biomaterialia*, **5**, 406-418 (2009).
13. Cooney, M. J.; Lau, C.; Windmeisser, M.; Liaw, B. Y.; Klotzbach, T.; Minteer, S. D., *Journal of Materials Chemistry*, **18**, 667-674 (2008).
14. Zhang, Y.; Gao, C.; Zhao, W.; Zhou, Z.; Yan, W.; Li, X.; Liu, Y.; Sun, Z.; Zhao, G.; Gao, J., *RSC Advances*, **4**, 33840-33847 (2014).
15. Orrego, C. E.; Valencia, J. S., *Bioprocess and Biosystems Engineering*, **32**, 197-206

(2009).

16. Xu, F.; Zhang, N.; Long, Y.; Si, Y.; Liu, Y.; Mi, X.; Wang, X.; Xing, F.; You, X.; Gao, J., *Journal of Hazardous Materials*, **188**, 148-155 (2011).
17. Okada, K.; Nandi, M.; Maruyama, J.; Oka, T.; Tsujimoto, T.; Kondoh, K.; Uyama, H., *Chemical Communications*, **47**, 7422-7424 (2011).
18. Zeng, X.; Ruckenstein, E., *Biotechnology Progress*, **15**, 1003-1019 (1999).
19. Park, S. B.; Fujimoto, T.; Mizohata, E.; Inoue, T.; Sung, M. H.; Uyama, H., *Journal of Microbiology and Biotechnology*, **23**, 942-952 (2013).
20. Ikeda, R.; Fujioka, H.; Nagura, I.; Kokubu, T.; Toyokawa, N.; Inui, A.; Makino, T.; Kaneko, H.; Doita, M.; Kurosaka, M., *International Orthopaedics*, **33**, 821-828 (2009).
21. Xin, Y.; Fujimoto, T.; Uyama, H., *Polymer (United Kingdom)*, **53**, 2847-2853 (2012).
22. Xi, F.; Wu, J., *Reactive and Functional Polymers*, **66**, 682-688 (2006).
23. Varshosaz, J.; Taymouri, S.; Hamishehkar, H., *Journal of Applied Polymer Science*, **131**(2014).
24. Xi, F.; Wu, J., *Journal of Chromatography A*, **1057**, 41-47 (2004).
25. Monier, M.; Ayad, D. M.; Wei, Y.; Sarhan, A. A., *Journal of Hazardous Materials*, **177**, 962-970 (2010).

Concluding remarks

In this doctoral thesis, EVOH-based monoliths with mesoporous structure and high surface area were fabricated. The monoliths were applied for various applications including SERS substrates, catalyst carrier, enzyme immobilization, and copper ions adsorption.

In Chapter 1, mesoporous EVOH monoliths were fabricated from the EVOH solution in a mixed solvent of IPA and water by TIPS. The morphology of the monoliths could be controlled by altering the fabrication conditions such as the cooling temperature and the concentration of EVOH. The resulting EVOH monoliths possessed large specific surface area and uniform mesoporous structure. In addition, the EVOH monoliths were successfully activated by CDI.

In Chapter 2, a unique method was developed for the generation of AgNPs embedded mesoporous EVOH monoliths. The existence of AgNPs was confirmed by TEM and EDX observation. The monoliths with uniformly dispersed AgNPs could detect MBA solution of low concentration (10^{-13} M). Moreover, the monoliths showed high Raman signal reproducibility toward MBA. Compared with conventional porous SERS substrates, which need complicated fabrication processes, the proposed method enabled facile one-pot fabrication of the substrates.

In Chapter 3, a one-pot method to fabricate PdNPs captured in mesoporous EVOH monoliths has been developed using TIPS method. The created PdNPs with diameters of 5-10 nm were dispersed uniformly in the PdNPs-EVOH monoliths. The XRD result showed the characteristic peaks of PdNPs. In addition, the monoliths demonstrated outstanding SMC catalytic performance toward various substrates. Furthermore, the monoliths exhibited low leaching property and high reusability.

In Chapter 4, catalase was immobilized onto the CDI activated EVOH monoliths. The immobilized catalase retained 75% of its initial activity after eleven successive cycles of decomposition of hydrogen peroxide. In addition, both the pH and temperature profiles of the free and immobilized catalase were confirmed. The immobilized catalase showed same maximum pH and temperature values to that of the free catalase. Moreover, the immobilized catalase exhibited better thermal stability than free catalase.

In Chapter 5, a monolithic material based on biocompatible EVOH and chitosan was fabricated by TIPS for the first time. The blend monolith showed mesoporous structure. FT-IR suggests the successful blend of the two polymers. The chitosan layer was interestingly located on the inner surface of the monoliths. Additionally, the blend monoliths showed good adsorption and desorption properties toward copper ions.

In conclusion, EVOH monoliths were successfully fabricated from the EVOH solution by TIPS technique using the unique affinity of EVOH toward IPA and water. The fabricated monoliths with interconnected porous structure have been applied for various applications. The monoliths will find applications in many other fields and contribute to the sustainable development.

List of publications

1. Mesoporous Poly(ethylene-*co*-vinyl alcohol) Monolith Captured with Silver Nanoparticles as a SERS Substrate: Facile Fabrication and Ultra-High Sensitivity

   Guowei Wang, Hiroyuki Yoshikawa, Eiichi Tamiya, Hiroshi Uyama

   RSC Advances, **5**, 25777 (2015).

2. One-Pot Fabrication of Palladium Nanoparticles Captured in Mesoporous Polymeric Monoliths and Their Catalytic Application in C-C Coupling Reactions

   Guowei Wang, Dhiman Kundu, Hiroshi Uyama

   Journal of Colloid and Interface Science, **451**, 184-188 (2015).

3. Reactive Poly(ethylene-*co*-vinyl alcohol) Monoliths with Tunable Pore Morphology for Enzyme Immobilization

   Guowei Wang, Hiroshi Uyama

   Colloid and Polymer Science, **293**, 2429 (2015).

4. Immobilization of Catalase onto Hydrophilic Mesoporous Poly(ethylene-*co*-vinyl alcohol) Monoliths

   Guowei Wang, Yuanrong Xin, Wenjuan Han, Hiroshi Uyama

   Journal of Applied Polymer Science, **132**, 42556 (2015).

5. Facile Fabrication of Mesoporous Poly(ethylene-*co*-vinyl alcohol)/Chitosan Blend Monoliths

   Guowei Wang, Yuanrong Xin, Hiroshi Uyama

   Carbohydrate Polymers, **132**, 345-350 (2015).

6. Novel Silver Nanoparticles-Embedded Porous Polymeric Film Coated on a Glass as a Biosensor Chip

   Guowei Wang, Hiroyuki Yoshikawa, Eiichi Tamiya, Hiroshi Uyama

   RSC Advances, in preparation.

Acknowledgments

This study was completed at the Department of Applied Chemistry, Graduate School of Engineering, Osaka University, from 2012 to 2015.

First and foremost, I would like to thank my supervisor Professor Hiroshi Uyama. Without his helpful and patient supervision, none of this research would be possible. The discussions with him always give me some hints and ideas for the research. He is not only an excellent professor but also a supporter to support many aspects of my lives in Japan. The strong scientific foundations that I have learned from him will guide my future career.

I am especially grateful to Assistant Professor Takashi Tsujimoto. His wisdom and experience in equipment helped me a lot. He is enthusiastic and always tries to dissolve almost every problem I have faced. I also want to express my appreciation to Assistant Professor Urara Hasegawa. She has good knowledge in biology and always gives me some valuable information.

I would like to thank Professor Tsuyoshi Inoue and Professor Takahiro Kozawa for their tremendous help in revising this thesis.

I greatly appreciate Professor Susumu Kuwabata and Assistant Professor Taro Uematsu for their kind helps with the ICP-AES measurements. I would like to thank Professor Nobuhito Imanaka and Associate Professor Shinji Tamura for XRD measurements.

I would like to appreciate Professor Eiichi Tamiya and Assistant Professor Hiroyuki Yoshikawa for SERS measurements.

I would like to thank Dr. André J van der Vlies and Dr. Yasushi Takeuchi. Both of them are kind, enthusiastic, and helpful. They are willing to help me whenever I approach them.

I am great appreciate to my previous and current colleagues in the lab: Dr.

Dhiman Kundu, Dr. Yuanrong Xin, Dr. Nao Hosoda, Dr. Sung-Bin Park, Dr. Wenjuan Han, Dr. Masaki Moriyama, Ms. Hyunhee Shim, Mr. Boxing Zhang, Mr. Tengjiao Wang, Mr. Zhibin Huang, Ms. Yu Shu, Mr. Tomonari Kanno, Ms. Hitomi Fukuda, Mr. Koichi Tamano, Mr. Qinghui Zhang, Mr. Keng Yao Tan, Ms. Jingyuan Niu, Ms. Xingyu Xiang, Mr. Jia Yu Chen, Ms. Hoi I Neng and all the members in Uyama laboratory.

I would like to show my great appreciation to my family members. They give me support and encouragement to persevere through setbacks. Their loves without reservation make me powerful to realize my dream.

July 2015

Guowei Wang